Laplacian Eigenfunctions in NMR. II. Theoretical Advances

DENIS S. GREBENKOV

Laboratoire de Physique de la Matière Condensée, CNRS-Ecole Polytechnique, F-91128 Palaiseau, France

ABSTRACT: In this article, theoretical advances in the study of restricted diffusion in NMR that have been achieved by using Laplacian eigenfunctions are described. The macroscopic signal is represented as the characteristic function of a random phase shift that a nucleus acquires during its motion in an inhomogeneous magnetic field. The moments of this random variable are written in a matrix form that is based on Laplacian eigenfunctions. This article focuses on the zeroth, first, and second moments which provide the major contribution to the macroscopic signal. The asymptotic behavior of the macroscopic signal in both short-time and long-time regimes is considered when the diffusion length is either much smaller or much larger than the size of a diffusion-confining domain, respectively. Apparent diffusion coefficient, localization regime, inverse spectral problem, and many other issues are discussed. © 2009 Wiley Periodicals, Inc. Concepts Magn Reson Part A 34A: 264–296, 2009.

KEY WORDS: Laplace operator; eigenfunction; eigenvalue; restricted diffusion; (reflected) Brownian motion; spin echo; gradient echo; confining domain; NMR; matrix formalism; heat kernel; diffusive propagator; asymptotic behavior

I. INTRODUCTION

A magnetic field is a superb experimental tool for encoding the motion of spin-bearing particles. When the particles are restricted by a porous medium, their motion is somehow altered that allows one to probe a geometrical structure of the medium. This is a basis for diffusion-weighted imaging (DWI) which found numerous applications in material sciences, geophysics, oil-recovery industry, biology and medical diagnostics, etc. DWI is successfully used for imaging various media, from mineral samples (e.g., cement, sandstones, clays, sedimentary rocks) to biological organs and tissues (e.g., brain, bone, lungs). In spite of outstanding experimental abilities provided by modern NMR scanners, many fundamental theoretical questions still bother both theoreticians and experimentalists. How does a geometrical restriction deviate the macroscopic signal from the classical Gaussian form which is known for unrestricted diffusion? Why does the surface-to-volume ratio of a confining medium appear in the short-time regime? What is the motional narrowing and how does it

Received 4 June 2009; revised 29 July 2009; accepted 5 August 2009

Correspondence to: Denis S. Grebenkov. E-mail: denis.grebenkov@polytechnique.edu

Concepts in Magnetic Resonance Part A, Vol. 34A(5) 264–296 (2009)

Published online in Wiley InterScience (www.interscience.wiley.com). DOI 10.1002/cmr.a.20145

change the signal at long times? What is an apparent diffusion coefficient and how can one measure it correctly? When and why does the Gaussian phase approximation fail to describe the macroscopic signal? Which theoretical models can replace it? What is the role of surface relaxation and how can one account for it? What are the limitations of the narrow-pulse approximation and is it possible to go beyond this frame? What information on a porous medium can be extracted from the macroscopic signal? How does the temporal profile (or gradient waveform) of an applied magnetic field influence the macroscopic signal? More generally, what is known about restricted diffusion and its role for nuclear magnetic resonance? A vast NMR literature is dedicated to answer these questions [see review (*1*) and references therein]. Here, a unified view on many of these questions by using Laplacian eigenfunctions is presented.

In Part 1, the focus was on Laplacian eigenfunctions as a basis for an efficient numerical tool (*2*). A deterministic description for the time evolution of a macroscopic magnetization was employed. The magnetization obeys a Bloch-Torrey equation that describes diffusion in a scalar field (a projection of an applied magnetic field). Laplacian eigenfunctions were used to reduce the Bloch-Torrey equation to a set of linear first-order differential equations. Its solution was given in terms of two governing matrices, Λ and $\mathcal{B}$ that represented the Laplace operator (matrix Λ) and an applied magnetic field (matrix $\mathcal{B}$). The macroscopic signal was written in a compact matrix form which is particularly suitable for numerical computations.

Moving a step further, this article explains how the matrices Λ and $\mathcal{B}$ can help to retrieve and extend many theoretical results about restricted diffusion. Here, a probabilistic description of microscopic dynamics of diffusing nuclei whose motion is modeled by reflected Brownian motion is given. Although this description is formally equivalent to the deterministic one, it gives an alternative insight onto restricted diffusion and turns out to be more appropriate for theoretical analysis. In a probabilistic framework, macroscopic quantities are represented as expectations of some functionals over random trajectories of individual particles. These Brownian trajectories are characterized by a diffusive propagator, whose eigenmode expansion yields compact spectral representations of macroscopic quantities.

In Section II, a reminder of basic facts about diffusion and its probabilistic interpretation is given. In Section III, multiple correlation functions are considered. The formulas for the moments of a random phase shift acquired by a nucleus, which diffuse in an inhomogeneous magnetic field are derived. This article focuses on the zeroth, first, and second moments which provide the major contribution to the macroscopic signal. Many classical results for both short-time and long-time regimes when the diffusion length is either much smaller or much larger than the size of a diffusion-confining domain, respectively, are retrieved and explained. Section IV is organized in the form of answers to some general or practical questions. The discussion concerns the meaning of an analytical solution, problems in modeling porous media, use and misuse of apparent diffusion coefficients, inverse spectral problem, etc. As in Part 1, the discussion is held on an intuitive level with many illustrations and examples. Further mathematical details and numerous references, as well as a historical overview, can be found in a review (*1*).

II. DIFFUSIVE MOTION

In this section, a reminder of basic facts about diffusion is given. They are as follows: microscopic dynamics and the central limit theorem; diffusive propagator; microscopic interpretation of boundary conditions; magnetic encoding and narrow-pulse approximation; notion of Laplacian eigenfunctions and eigenvalues; asymptotic regimes. An experienced reader can skip this section which provides an alternative and complementary presentation, from the probabilistic point of view, of the notions that had already been discussed in Section II of Part 1 (*2*).

Microscopic Dynamics

Since the first observation reported by the British botanist Robert Brown (*3*), diffusion is acknowledged as a fundamental transport mechanism. In Brown's experiment, pollens of Clarkia are submerged in water in which they are permanently "bombarded" by water molecules. In a dilute suspension, the encounters between pollens are rare so that their dynamics can be considered as mutually independent. The number of the surrounding water molecules is very large, while their individual actions on the pollen are tiny and (almost) uncorrelated. As a consequence, microscopic displacements of each pollen are not deterministic (as the motion of planets), but random. The randomness emerges here as a lack of information or a practical impossibility to survey a huge number of individual water molecules. The randomness means that a pollen, started at time 0 from a point $\mathbf{r}_0$, can be found in whatever place in space at a later time t (throughout the text, vectors and points in

space are written in bold). Although the precise location $\mathbf{r}$ of a given pollen at time t cannot be predicted, it can be characterized by a probability density that describes how likely it is for the pollen to be at $\mathbf{r}$. As probability can also be interpreted as the frequency of occurence of some event (e.g., displacement of a pollen from $\mathbf{r}_0$ to $\mathbf{r}$), the probability density for a single pollen is proportional to a macroscopic (physical) density of many independent (noninteracting) pollens. As each pollen follows its own microscopic dynamics, its trajectory can be seen as an independent realization of the underlying stochastic process.

After hitting a pollen, water molecules quickly return to their thermal equilibrium and loose the memory of their action. The corresponding decorrelation time τ is many orders of magnitude smaller than a macroscopic observation time t. The displacements $\mathbf{r}_i$ of a pollen at the microscopic time scale τ are therefore (almost) independent random variables, typically with zero mean and small finite variance σ^2. The resulting macroscopic displacement W_t at time t is the sum of a large number $N = t/\tau$ of small displacements $\mathbf{r}_i$. Although the average displacement is still zero, stochastic fluctuations around this value are of the order of $\sigma\sqrt{N}$. In fact, the mean square displacement at time t is

$$\mathbb{E}\{W_t^2\} = \mathbb{E}\left\{\left(\sum_{i=1}^{N} \mathbf{r}_i\right)^2\right\} = \sum_{i,j=1}^{N} \mathbb{E}\{\mathbf{r}_i \mathbf{r}_j\},$$

where $\mathbb{E}$ denotes the expectation (or an average). If any two displacements $\mathbf{r}_i$ and $\mathbf{r}_j$ are independent, then $\mathbb{E}\{\mathbf{r}_i \mathbf{r}_j\} = \mathbb{E}\{\mathbf{r}_i\}\mathbb{E}\{\mathbf{r}_j\} = 0$ since $\mathbb{E}\{\mathbf{r}_i\} = 0$. The contributions come from the terms with $i = j$:

$$\mathbb{E}\{W_t^2\} = \sum_{i=1}^{N} \mathbb{E}\{\mathbf{r}_i^2\} = N\sigma^2.$$

The square root of the left-hand side of this equation characterizes fluctuations. Replacing N by t/τ yields the Einstein's relation

$$\mathbb{E}\{W_t^2\} = 2dDt, \quad \text{with } D = \frac{\sigma^2}{2d\tau}, \qquad [1]$$

d being the dimension of space. The diffusion coefficient D, a macroscopic transport parameter, naturally appears here as the ratio between two relevant characteristics of the microscopic dynamics: σ^2 and τ. Diffusion turns out to be an effective description of a complex microscopic dynamics at macroscopic time scales.

The above elementary analysis can be substantially refined. For this purpose, one can use the central limit theorem that gives a precise probabilistic description of fluctuations. The theorem states that the macroscopic displacements of a pollen are distributed according to the normal (or Gaussian) law (*4*). In mathematical terms, the probability that a pollen which started at time 0 from a point $\mathbf{r}_0$ arrives at time t in a vicinity of a point $\mathbf{r}$ is described by the following density:

$$G_t(\mathbf{r}_0, \mathbf{r}) = (4\pi Dt)^{-d/2} \exp\left[-\frac{(\mathbf{r}_0 - \mathbf{r})^2}{4Dt}\right]. \qquad [2]$$

The Gaussian integral

$$\int_{-\infty}^{\infty} dx\, e^{-ax^2} = \sqrt{\pi/a} \quad (a > 0)$$

allows one to check the correct normalization of the probability density $G_t(\mathbf{r}_0,\mathbf{r})$:

$$\int_{\mathbb{R}^d} d\mathbf{r}\, G_t(\mathbf{r}_0, \mathbf{r}) = 1,$$

where $\mathbb{R}^d$ denotes d-dimensional space.

In addition, one can use Eq. [2] to retrieve the moments of Brownian motion W_t, for instance,

$$\mathbb{E}\{W_t\} = \int_{\mathbb{R}^d} d\mathbf{r}\, \mathbf{r}\, G_t(0, \mathbf{r}) = 0$$

$$\mathbb{E}\{W_t^2\} = \int_{\mathbb{R}^d} d\mathbf{r}\, \mathbf{r}^2\, G_t(0, \mathbf{r}) = 2dDt, \qquad \text{etc.}$$

(assuming that Brownian motion started from the origin).

The probability density $G_t(\mathbf{r}_0,\mathbf{r})$ describing diffusion between two points is often called a diffusive propagator, a heat kernel or the Green function of a diffusion equation. In deterministic dynamics, a natural question to ask is "Where does a particle arrive at a given time?". This question has to be adapted to the intrinsic uncertainty of Brownian dynamics, for which it can be reformulated as follows "With which probability does a particle arrive at a given location at a given time?". The role of a propagator is precisely to answer this question.

Whatever the probability distribution of the independent finite-variance microscopic displacements $\mathbf{r}_i$ is, the diffusion coefficient D remains the only relevant information at a macroscopic level, while all other details of the microscopic dynamics are aver-

aged out. In other words, the Gaussian character of macroscopic displacements appears without any specific knowledge of microscopic interactions. This is one of the reasons why diffusion is so ubiquitous in nature and sciences. It is worth stressing, however that the uncorrelated character of interactions and the finite variance of displacements are two important conditions for using the central limit theorem. Although these conditions can be weakened, if either of them is not respected, it may result in anomalous diffusions, for which Eqs. [1,2] do not hold [see (*5–9*) and references therein].

In Part 1, a diffusion equation was established first and Eq. [2] for a propagator was then obtained as its solution. In this article, Eq. [2] is a direct consequence of the central limit theorem, while it is easy to check that $G_t(\mathbf{r}_0,\mathbf{r})$ satisfies the diffusion equation

$$\frac{\partial}{\partial t}G_t(\mathbf{r}_0,\mathbf{r})-D\Delta G_t(\mathbf{r}_0,\mathbf{r})=0, \qquad [3]$$

where $\Delta=\partial^2/\partial x_1^2+\cdots+\partial^2/\partial x_d^2$ is the Laplace operator acting on $\mathbf{r}=(x_1,\ \ldots\ x_d)$. This equation describes the time evolution of the probability density $G_t(\mathbf{r}_0,\ \mathbf{r})$ from an initial condition with a point-like source:

$$G_{t=0}(\mathbf{r}_0,\mathbf{r})=\delta(\mathbf{r}-\mathbf{r}_0), \qquad [4]$$

$\delta(\mathbf{r}_0-\mathbf{r})$ being the Dirac distribution. Although Brownian trajectories are random, the probability density $G_t(\mathbf{r}_0,\ \mathbf{r})$ satisfies a deterministic equation. At time $t=0$, a particle is localized at $\mathbf{r}_0$ so that $G_{t=0}(\mathbf{r}_0,\mathbf{r})=0$ for all $\mathbf{r}\neq\mathbf{r}_0$. In the course of time, the particle explores further and further regions around the starting point $\mathbf{r}_0$ that "spreads" the probability density. The "spreading" is characterized by the diffusion length $\sqrt{\mathbb{E}\{W_t^2\}/2d}=\sqrt{Dt}$.

The propagator $G_t(\mathbf{r}_0,\mathbf{r})$ is invariant under the permutation of the starting and arrival points:

$$G_t(\mathbf{r}_0,\mathbf{r})=G_t(\mathbf{r},\mathbf{r}_0). \qquad [5]$$

This symmetry reflects the invariance of the statistical properties of Brownian trajectories under the time reversal: the probability for coming from $\mathbf{r}_0$ to $\mathbf{r}$ is equal to the probability for coming from $\mathbf{r}$ to $\mathbf{r}_0$.

A diffusive propagator, an "elementary brick" in the description of translational dynamics, can be used for an explicit construction of a solution to a diffusion problem. For instance, if $\rho(\mathbf{r}_0)$ is an initial density of particles (conventionally normalized to 1), the density of particles at time t, $c(\mathbf{r},t)$, is simply a linear superposition of solutions with a fixed starting point:

$$c(\mathbf{r},t)=\int d\mathbf{r}_0\ \rho(\mathbf{r}_0)\ G_t(\mathbf{r}_0,\mathbf{r}).$$

In probabilistic terms, $d\mathbf{r}_0\ \rho(\mathbf{r}_0)$ is the probability for choosing the starting point $\mathbf{r}_0$, while $G_t(\mathbf{r}_0,\mathbf{r})$ describes the diffusive motion from $\mathbf{r}_0$ to $\mathbf{r}$.

The central limit theorem guarantees that any microscopic dynamics (with uncorrelated finite-variance "elementary steps") could be described by a diffusion equation at macroscopic time and length scales. This statement allows one to substitute complex microscopic dynamics by much simpler ones:

- a lattice random walk, that is a discrete Markov process (without memory) which consists in successive independent random "jumps" of a particle between adjacent sites of a graph (e.g., neighboring sites of a square lattice) (*10–12*);
- Brownian motion (or Wiener process) which is a continuous stochastic process with independent Gaussian increments (*4*, *13*); in this case, the probability density [2] describes all the moves of a particle, even at microscopic scales.

Although these two stochastic processes are different from each other, *and from the microscopic dynamics of real atoms or molecules*, they lead to the same macroscopic description via diffusion equation. This is the reason for using random walks and Brownian motion for a theoretical analysis and a numerical modeling of microscopic dynamics at macroscopic scales.

Boundary Condition

In most practical situations, particles are confined in a reservoir that is called here a diffusion-confining domain Ω. This is the case for water molecules in cells and tissues, hydrocarbon molecules (oil) in sedimentary rocks, oxygen molecules in the lungs, etc. When the motion of particles is restricted inside a domain Ω, microscopic interactions between particles and a boundary should be taken into account. These are usually short-range interactions that occur in a thin surface layer near the boundary $\partial\Omega$ of the domain Ω. Examples are widespead in physics, chemistry, and biology, for instance:

1. magnetic impurities distributed on the interface may destroy the transverse magnetization of a nucleus near the boundary;
2. a chemical reaction on a catalytic surface transforms one species to the others that

modifies the concentration of the former species;
3. a semipermeable interface allows for particles to escape from a diffusion-confining domain, etc.

If the contact with the boundary is short in comparison with macroscopic time scales, a precise description of underlying physicochemical or biological interactions becomes irrelevant. The surface layer can therefore be treated as a "black box": after a short time τ, one of the two opposite events occurs with a particle which arrived onto the boundary:

- with some sticking probability $1 - \varepsilon$, the particle changes its state (either by losing magnetization on a magnetic impurity, or by absorption, transfer, or chemical transformation) and does not participate in the transport process anymore;
- or, with probability ε, the particle is somehow "released" to the outside of the surface layer (at some distance in the order of σ); in other words, the diffusive motion is resumed in a vicinity of the hitting point and continued in the bulk.

The specific nature of interactions determines the values (or probability distributions) for the τ and σ. The boundary parameters (adsorption, interaction or waiting time τ, and surface layer width σ) are often identified with, or confused with, the bulk parameters from "Microscopic Dynamics" section (decorrelation time τ and the standard deviation σ). Although such identification is not rigorous, the smallness of these microscopic characteristics in comparison with observation time and length scales may justify this kind of approximation.

When a boundary is purely absorbing (no reflections, $\varepsilon = 0$), so that the concentration of particles on this boundary is equal to 0. This is incorporated into macroscopic description through a Dirichlet boundary condition: $G_t(\mathbf{r}_0, \mathbf{r}) = 0$ when $\mathbf{r} \in \partial\Omega$. This condition can also be understood as zero probability for arriving from a boundary point $\mathbf{r}$ to another point $\mathbf{r}_0$ (because of immediate absorption at $\mathbf{r}$).

In the opposite limit of a purely reflecting boundary (no absorptions, $\varepsilon = 1$), no particle can cross the boundary so that the flux of particles across the boundary is equal to 0. This is incorporated through a Neumann boundary condition: $\partial G_t(\mathbf{r}_0, \mathbf{r})/\partial n = 0$ when $\mathbf{r} \in \partial\Omega$. Here $\partial/\partial n$ is the normal derivative, acting on $\mathbf{r}$ and pointing toward the exterior of a domain. The normal derivative is the projection of the gradient operator $\bigtriangledown$ onto the unit vector $\mathbf{n}(\mathbf{r})$ which is orthogonal to the boundary at point $\mathbf{r}$. For instance, if the domain is a sphere, the normal derivative $\partial/\partial n$ coincides with the radial derivative $\partial/\partial r$.

For the intermediate case $0 < \varepsilon < 1$, absorptions and reflections are chosen randomly with probabilities $1 - \varepsilon$ and ε, respectively. Such a partially absorbing or partially reflecting boundary is represented by a linear combination of Dirichlet and Neumann boundary conditions:

$$D\frac{\partial}{\partial n}G_t(\mathbf{r}_0, \mathbf{r}) + K\,G_t(\mathbf{r}_0, \mathbf{r}) = 0 \quad (\mathbf{r} \in \partial\Omega). \quad [6]$$

The above Robin (also known as Fourier, mixed, relaxing, radiation, or third) boundary condition should be satisfied for any starting point $\mathbf{r}_0$. The balance between reflections and absorptions in Eq. [6] is controlled by macroscopic transport coefficients D and K, the latter bearing different names: surface relaxivity, permeability of a membrane, reactivity of a catalyst, absorption rate for trapping processes, etc. As the diffusion coefficient D represents a combination of microscopic bulk parameters according to Eq. [1], the surface relaxivity K accounts for the microscopic surface parameters (*14*):

$$K = \frac{\sigma}{2d\tau}\frac{1-\varepsilon}{\varepsilon}.$$

The transport coefficients D and K are in units of square meter per second and meter per second, respectively, their ratio D/K being homogeneous to a length. This so-called unscreened perimeter length plays an important role in diffusive transport phenomena (*15–22*). The inverse of this length is normalized by the size L of a diffusion-confining domain for getting a dimensionless parameter

$$h = \frac{KL}{D}. \quad [7]$$

The presence of a boundary condition substantially modifies a solution of the diffusion equation [3]. In particular, the propagator from Eq. [2] for the whole space does not satisfy the boundary condition [6] in any bounded domain. In other words, each confining domain has its own diffusive propagator that depends on the transport parameters D and K.

Reflected Brownian Motion. The presence of a boundary drastically affects the mathematical construction of Brownian motion. In a probabilistic description, a Dirichlet boundary condition is easily

implemented by introducing a stopping (or hitting) time $\mathbb{T}$ (*23*). This is the first (random) moment when Brownian motion which started inside a confining domain encounters its boundary. As a particle having encountered the boundary should be immediately absorbed, it is sufficient to consider the diffusive process for times t between 0 and $\mathbb{T}$. In other words, we simply close our eyes to what happens after the first contact. A geometrical restriction is fully introduced through the stopping time $\mathbb{T}$, while Brownian motion remains unchanged. This fact is crucial for many computational aspects.

However Dirichlet boundary condition (or purely absorbing surfaces) is rarely encountered in NMR. In most experimental situations, magnetic impurities which are distributed on the boundary have a finite relaxation rate that corresponds to partially absorbing/reflecting surfaces (Robin boundary condition). In the special case of zero relaxation rate, one may deal with purely reflecting surfaces (Neumann boundary condition). In both cases, ordinary Brownian motion is not appropriate. This is intuitively clear: once a particle encounters a boundary, it is "forced" to remain inside the diffusion-confining domain, while ordinary Brownian motion is free to leave the domain. We have therefore to modify the local dynamics of the process in order to include reflections on the boundary. In contrast to (ordinary) Brownian motion, the construction of such a stochastic process, known as "reflected Brownian motion," strongly depends on the geometry of a confining medium. For smooth boundaries, reflected Brownian motion is defined as a solution of a stochastic differential equation known as the Skorokhod Equation (*13*):

$$dX_t = dW_t + \mathbf{n}(X_t)\mathbb{I}_{\partial\Omega}(X_t)d\ell_t, \qquad [8]$$

where W_t is the (ordinary) Brownian motion, $\mathbb{I}_{\partial\Omega}(\mathbf{r})$ is the indicator function of the boundary [$\mathbb{I}_{\partial\Omega}(\mathbf{r}) = 1$ if $\mathbf{r}$ belongs to $\partial\Omega$, and 0 otherwise], and ℓ_t is the boundary local time, satisfying certain conditions [see (*13*) for details]. The most unusual feature of the above definition is that a single equation defines two processes, X_t and ℓ_t, both strongly dependent on each other. The intuitive meaning of the Skorokhod equation is simple. Inside a diffusion-confining domain, an infinitesimal variation dX_t of reflected Brownian motion X_t is governed uniquely by the variation dW_t of the (ordinary) Brownian motion W_t because the second term in Eq. [8] vanishes due to the indicator function $\mathbb{I}_{\partial\Omega}$. When a particle hits the boundary, the presence of the second term does not allow the particle to leave the domain. In fact, this term leads to a variation directed along the inward unit normal $\mathbf{n}(\mathbf{r})$ toward the interior of the domain. At the same time, each encounter with the boundary increases the boundary local time ℓ_t. Reflected Brownian motion can alternatively be introduced as a continuous limit of reflected random walks on a regular lattice, which are easier for intuitive interpretation (*24*, *25*). The Robin boundary condition (partial absorption/reflection) can also be implemented for reflected Brownian motion by putting a special stopping condition (*21*, *22*). A further discussion of these issues goes beyond the scope of this article.

Independently of the way how reflected Brownian motion is constructed, a diffusive propagator $G_t(\mathbf{r}_0,\mathbf{r})$ satisfying Eqs. [3,4,6] is the probability density for (partially) reflected Brownian motion for moving from $\mathbf{r}_0$ to $\mathbf{r}$ during time t inside a diffusion-confining domain Ω with a partially absorbing/reflecting boundary $\partial\Omega$. In what follows, the propagator $G_t(\mathbf{r}_0,\mathbf{r})$ is used as an "elementary brick" in the description of translational dynamics.

Magnetic Field Encoding

Experimental observation of translational dynamics requires a kind of "marking" or "labeling" of traveling particles for tracking their displacements in space. In some cases, one can monitor individual displacements of diffusing particles by using a colored liquid, radioactive isotopes, fluorescent particles, magnetic contrast agents, etc. Such single-particle imaging techniques may however be difficult, expensive, or undesired. For instance, if one is interested in water activity in a cell, one needs to "label" all water molecules according to their spatial positions in the system (like runners in a stadium are numbered according to their lanes). A magnetic field is a superb experimental tool for encoding positions and whole trajectories of spin-bearing particles (e.g., protons of water molecules) (*26*, *27*).

A Qualitative Picture. To get a qualitative picture of a spin-echo magnetic field encoding, one can imagine a river flowing between two parallel banks along the x axis. The flow velocity $v(y)$ is smaller near the banks and larger in the middle (Fig. 1). At time $t = 0$, one releases a colored stain in the shape of a vertical segment at $x = 0$. Because the velocity is different in various streamlines, the initial linear segment is getting distorted as $x(y) = v(y)t$. At time $t = T/2$, the flow direction is instantly reversed, so that the velocity profile becomes $-v(y)$. The colored stain completely recovers its original shape of a linear segment at time $t = T$.

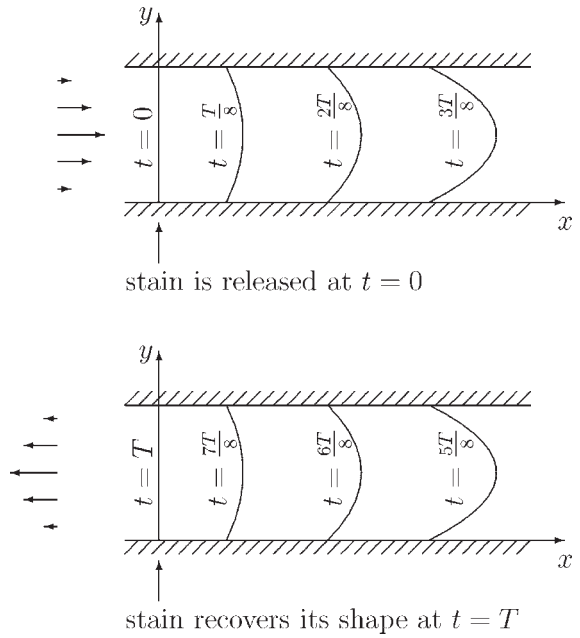

Figure 1 Illustration for a recovery of the colored stain's original shape in a laminar flow. At time $t = 0$, a colored stain in the shape of a vertical segment is released in a flow with a given velocity profile $v(y)$. The original linear profile is gradually distorted as the particles move with different velocities depending on the height y of their streamline. At time $t = T/2$, the flow is reversed [the velocity profile becomes $-v(y)$] that leads to a recovery of the stain's original shape at time $t = T$.

This simplified picture does not account for diffusion. Diffusion in the longitudinal direction (x axis) would blur the recovered shape, independently of the velocity. Diffusion in the transverse direction (y axis) allows the particles to move from one streamline to the other. This phenomenon, known as Taylor dispersion, damages or fully destroys the original shape. The position $x(t)$ is no longer determined by the initial height y, but by the whole Brownian trajectory $y(t)$:

$$x(t) = \int_0^t dt' v(y(t'), t')$$

so that $x(t)$ is a random variable which depends on the velocity profile (*28*).

The transverse dispersion mechanism in flow is very similar to magnetic field encoding when the nuclei diffuse between spatial regions with different Larmor frequencies (angular velocities). In fact, a 90° radio frequency (rf) pulse turns the magnetization of nuclei into the transverse plane which is perpendicular to the orientation of the magnetic field (conveniently, the z axis) (*29*). In a constant magnetic field B_0 oriented along the z axis, the magnetization precesses around the z axis with the Larmor frequency γB_0, γ being the gyromagnetic ratio (a fundamental constant of a nucleus). Thinking of the transverse plane xy as a complex plane, one can introduce the complex-valued magnetization $\mathfrak{m} = \mathfrak{m}_x - i\mathfrak{m}_y$, i being the imaginary unit. If the absolute value of $\mathfrak{m}$ remains constant (no transverse relaxation), the magnetization $\mathfrak{m}$ is fully determined by the phase $\varphi = \gamma B_0 t$ acquired up to time t: $\mathfrak{m} \propto e^{i\varphi}$. Note that if the magnetization was defined as $\mathfrak{m} = \mathfrak{m}_x + i\mathfrak{m}_y$, the sign minus would appear in front of the phase ϕ: $\mathfrak{m} \propto e^{-i\varphi}$.

When the applied magnetic field is not constant, the acquired phase can be obtained by integrating the Larmor frequency $\gamma B(\mathbf{r},t)$ along the trajectory $\mathbf{r}(t)$ of a nucleus up to the observation time T:

$$\varphi = \int_0^T dt\ \gamma B(\mathbf{r}(t), t), \qquad [9]$$

where a scalar field $B(\mathbf{r},t)$ is the magnetic field applied along the z axis (which is perpendicular to the transverse plane xy). Taking a small time step τ, one can think of this integral as a sum of "elementary" phase shifts $\tau\ \gamma\ B(\mathbf{r}_k, k\tau)$, acquired at successive positions $\mathbf{r}_k = \mathbf{r}(k\tau)$ of the nucleus along its trajectory $\mathbf{r}(t)$. For a chosen magnetic field $B(\mathbf{r},t)$, Eq. [9] defines a functional which associates a (total) phase shift φ to a Brownian trajectory $\mathbf{r}(t)$. The phase shift φ is therefore a random variable. Its probability distribution can characterize the translational dynamics of spin-bearing particles.

In contrast to single-particle imaging, pulsed-gradient NMR techniques do not monitor individual trajectories but intrinsically rely on statistical information about the whole ensemble of spin-bearing particles. It is a challenge for a theoretician to develop appropriate mathematical tools for interpreting this information in the most efficient way.

Although the scalar field $B(\mathbf{r},t)$ is introduced as a magnetic field, its role as a weighting function of reflected Brownian motion in Eq. [9] is much more general and it goes far beyond NMR. In general, the function $B(\mathbf{r},t)$ can be thought of as a distribution of "markers" for distinguishing points and regions of a diffusion-confining domain. When a particle diffuses, the random variable φ accumulates the corresponding "marks" along the particle trajectory $\mathbf{r}(t)$. Each point of the trajectory is thus weighted according to $B(\mathbf{r}(t),\ t)$, which "encodes" the whole trajectory through a single random number, the random variable φ. The function $B(\mathbf{r},t)$ may represent various encoding mechanisms besides a magnetic field. For example, if the bulk contained absorbing sinks or relaxing impurities, $B(\mathbf{r},t)$ would represent the distribution of absorption or relaxation rates. Here, φ

would be a cumulant absorption factor penalizing the trajectories which pass through the sinks (*30*).

Probabilistic Description. The microscopic magnetization of individual nuclei form a macroscopic signal E which can be measured in a diffusion-weighted experiment:

$$E = \mathbb{E}\{e^{i\varphi}\}, \qquad [10]$$

where an average over the ensemble of nuclei is replaced by the expectation $\mathbb{E}$ over all Brownian trajectories $\mathbf{r}(t)$ inside a diffusion-confining domain. Here, we omit a proportionality factor between the macroscopic signal (an experimentally measurable current induced in a receiver by rotating magnetization of nuclei) and the expectation in the right-hand side of Eq. [10]. Although many diffusive NMR phenomena are fully described by apparently simple and intuitively clear equations [9, 10], the diversity and complexity of these phenomena are caused by intricate properties of reflected Brownian motion (*13*, *21*).

Rigorously speaking, one should specify a kind of Brownian trajectories to take into account in Eq. [10]. For this purpose, the conditional expectation of the transverse magnetization $e^{i\varphi}$ is introduced,

$$\mathrm{M}(\mathbf{r}_0,\mathbf{r},T)d\mathbf{r} = \mathbb{E}\{e^{i\varphi}|\mathbf{r}(0)=\mathbf{r}_0,\mathbf{r}(T)=\mathbf{r}\}, \qquad [11]$$

over all the trajectories of reflected Brownian motion which started from $\mathbf{r}_0$ at time 0 and arrived to $\mathbf{r}$ at time T. This quantity should not be confused with the propagator $G_t(\mathbf{r}_0,\mathbf{r})$ that can be written in a similar form in which $e^{i\varphi}$ is replaced by 1. The "density" $\mathrm{M}(\mathbf{r}_0, \mathbf{r}, T)$ is the contribution to the macroscopic signal from the nuclei started from $\mathbf{r}_0$ and arrived to $\mathbf{r}$. If $\rho(\mathbf{r}_0)$ is the initial density of nuclei (normalized to 1), $d\mathbf{r}_0\rho(\mathbf{r}_0)$ can be interpreted as a probability for choosing the starting point $\mathbf{r}_0$. The magnetization at time T is an average over all starting points:

$$\mathrm{m}(\mathbf{r},T) = \int_\Omega d\mathbf{r}_0\rho(\mathbf{r}_0)\mathrm{M}(\mathbf{r}_0,\mathbf{r},T). \qquad [12]$$

The macroscopic signal is determined by weighting the contributions from the nuclei arrived to $\mathbf{r}$, by a sampling or pickup function $\tilde{\rho}(\mathbf{r})$ of a receiver (coil or antenna):

$$E = \int_\Omega d\mathbf{r}\ \mathrm{m}(\mathbf{r},T)\tilde{\rho}(\mathbf{r}). \qquad [13]$$

The function $\tilde{\rho}(\mathbf{r})$ may account for nonuniform spatial characteristics of a receiver, as well as for voxel locations in diffusion-weighted imaging. In most cases, $\tilde{\rho}(\mathbf{r})$ is assumed to be a constant. Note that Eq. [10] is a shorter form of Eqs. [11–13].

In a probabilistic language, the magnetization $\mathfrak{m}(\mathbf{r},T)$ and the macroscopic signal E are expectations of a functional of the phase shift φ in Eq. [9]. At the same time, the magnetization $\mathfrak{m}(\mathbf{r},T)$ was introduced in Part 1 as a solution of the Bloch-Torrey equation (*31*). Similarly, the conditional expectation $\mathrm{M}(\mathbf{r}_0, \mathbf{r}, T)$ turns out to be the Green function of the Bloch-Torrey equation. Deep connections between Brownian motion and second-order partial differential equations have many important consequences and bring instructive and complementary insights onto restricted diffusion. For instance, the integral representation [13] of the characteristic function in Eq. [10] is known as Feynman-Kac formula (*13*, *32–34*). It provides a link between the probabilistic and PDE descriptions used here and in Part 1, respectively.

Narrow-Pulse Approximation. A probabilistic description through Eqs. [9,10] is a general mathematical basis for studying diffusion in a magnetic field. In spite of a deceptive simplicity of Eqs. [9,10], finding the macroscopic signal is a difficult task. An NMR community is more used to a simpler description known as narrow-pulse approximation (NPA) which was proposed by Tanner and Stejskal (*35*). Although the general case for a given magnetic field $B(\mathbf{r},t)$ was mathematically untractable at that time, the choice for using a particular magnetic field was at experimentalist's hands. Can one choose the specific magnetic field $B(\mathbf{r},t)$ for which the problem becomes solvable? Tanner and Stejskal proposed to apply two short gradient pulses for encoding the starting and arrival positions of spin-bearing particles (Fig. 2). During a gradient pulse, the nuclei gain phase shifts that depend on their positions. A phase shift plays a role of a spatial label for each nucleus. Since the particles move randomly, independently of each other, and regardless of their spatial labels, the initial spatially ordered arrangement of labels is gradually destroyed in the course of time. At the observation time, the initial labels have to be compared with the current positions of particles. For this purpose, another gradient pulse of opposite polarity is applied (this is analogous to inverting the flow direction in our qualitative picture). None of the initial labels exactly match the current ones. The difference between initial and final positions of each particle, being depended on its whole trajectory, is random. On average, however, faster diffusion is expected to yield larger differences. The probability distribution of the phase shifts can thus characterize the translational dynamics of spin-bearing particles.

In mathematical terms, a phase shift due to Tanner-Stejskal short gradient pulses is

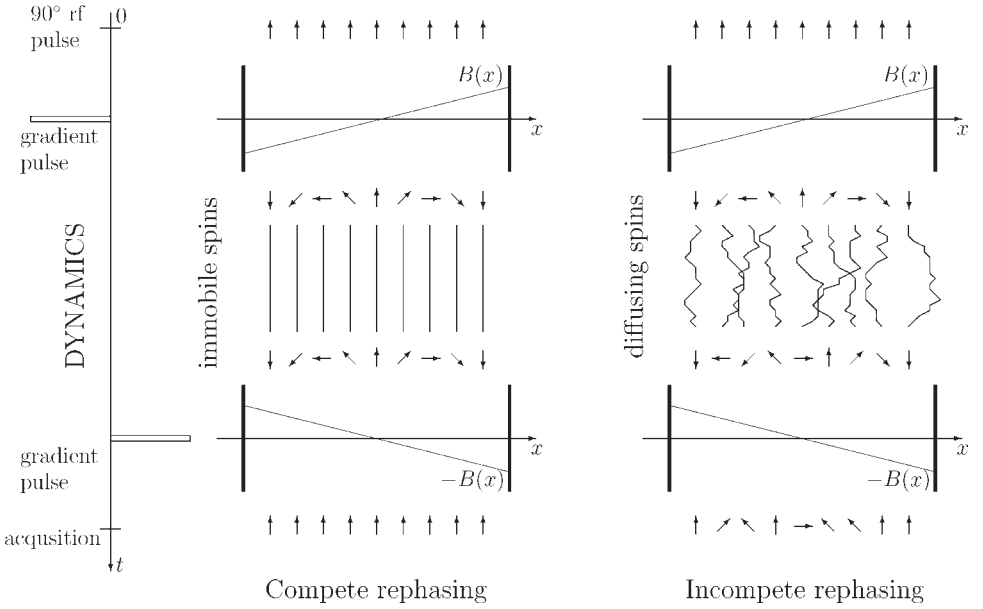

Figure 2 Encoding the positions of spin-bearing particles by two short-time gradient pulses. A 90° rf pulse flips all spins into the transverse plane, in which they rotate in phase, independently of their positions between two parallel plates (shown as thick vertical segments). During the first gradient pulse, $B(x) = gx$, each spin gains a phase shift $\gamma g x \delta$ depending on its position x along the direction of the applied gradient. This phase shift plays a role of a spatial label for the spin. For an acquisition, another gradient pulse of opposite direction, $B(x) = -gx$, is applied before observation time T. If spins were immobile (on the left), the net dephasing would be zero for all of them. In other words, the rephasing by the second gradient pulse would be complete, allowing to form an echo (macroscopic signal). On the right, the spin-bearing particles diffuse that is schematically represented by broken lines. Since the arrival positions do not match the initial positions (encoded spatial labels), the rephasing is not complete. An echo still appears, but its amplitude is attenuated. The probability distribution of phase shifts can thus characterize the dynamics of spin-bearing particles through the spin-echo attenuation.

$$\varphi = \int_0^{\delta} dt\, \gamma B(\mathbf{r}(t)) - \int_{T-\delta}^{T} dt\, \gamma B(\mathbf{r}(t)) \simeq \gamma\delta[B(\mathbf{r}(0)) - B(\mathbf{r}(T))]. \qquad [14]$$

Since the motion of particles between times δ and $T - \delta$ is not affected by a magnetic field, the translational dynamics is described by a diffusive propagator $G_t(\mathbf{r}_0,\mathbf{r})$:

$$\mathrm{M}(\mathbf{r}_0,\mathbf{r},T) \simeq e^{i\gamma\delta[B(\mathbf{r}_0)-B(\mathbf{r})]} G_T(\mathbf{r}_0,\mathbf{r}),$$

and the macroscopic spin-echo signal at time T is

$$E = \int_\Omega \underbrace{d\mathbf{r}_0\, \rho(\mathbf{r}_0)}_{\substack{\uparrow \\ \text{choosing starting point } \mathbf{r}_0}} \underbrace{e^{i\gamma\delta B(\mathbf{r}_0)}}_{\substack{\uparrow \\ \text{encoding starting point } \mathbf{r}_0}} \int_\Omega \underbrace{d\mathbf{r}\, G_T(\mathbf{r}_0,\mathbf{r})}_{\substack{\uparrow \\ \text{diffusing from } \mathbf{r}_0 \text{ to } \mathbf{r}}} \underbrace{e^{-i\gamma\delta B(\mathbf{r})}}_{\substack{\uparrow \\ \text{encoding arrival point } \mathbf{r}}}$$

averaging over starting points — averaging over arrival points

where the sampling function $\tilde{\rho}(\mathbf{r})$ was assumed to be constant. A probabilistic reading of this formula is explicit (Fig. 2). In fact, one first chooses randomly a particle at point $\mathbf{r}_0$ (with probability $\rho(\mathbf{r}_0)d\mathbf{r}_0$) and encodes its position by the first gradient pulse (the first exponential). Up to time T, the particle diffuses to a random point $\mathbf{r}$ with probability $G_t(\mathbf{r}_0,\mathbf{r})d\mathbf{r}$, where it gets another phase shift due to the second gradient pulse represented by the second exponential. The macroscopic signal at time T is formed by the whole ensemble of particles so that all possible starting positions $\mathbf{r}_0$ and arrival positions $\mathbf{r}$ have to be averaged (the two integrals).

In most cases of practical interest, an inhomogeneous magnetic field $B(\mathbf{r})$ is generated with a linear gradient g in a given spatial direction $\mathbf{e}$, $B(\mathbf{r}) = g(\mathbf{e} \cdot \mathbf{r})$. Assuming a uniform initial density, $\rho(\mathbf{r}) = 1/V$, and denoting $\mathbf{k} = \gamma g \delta \mathbf{e}$, one gets

$$E = \frac{1}{V} \int_\Omega d\mathbf{r}_0 \int_\Omega d\mathbf{r}\, G_T(\mathbf{r}_0,\mathbf{r}) e^{i\mathbf{k}(\mathbf{r}_0-\mathbf{r})}, \qquad [15]$$

where V is the volume of a diffusion-confining domain Ω. The macroscopic signal as a function of $\mathbf{k}$ appears as a kind of Fourier transform of the propa-

gator $G_t(\mathbf{r}_0,\mathbf{r})$. In fact, if the diffusive propagator $G_t(\mathbf{r}_0,\mathbf{r})$ is formally extended to the whole space $\mathbb{R}^d$ by putting $G_t(\mathbf{r}_0,\mathbf{r}) = 0$ whenever $\mathbf{r}_0$ or $\mathbf{r}$ is outside of the confining domain Ω, the above integrals can be written as

$$E = \frac{1}{V}\int\limits_{\mathbb{R}^d} d\mathbf{r}\, e^{-i\mathbf{k}.\mathbf{r}} \left[\int\limits_{\mathbb{R}^d} d\mathbf{r}_0\; G_T(\mathbf{r}_0, \mathbf{r}_0 + \mathbf{r})\right].$$

In experiment, the direction and amplitude of the vector $\mathbf{k}$ are varied to assess the averaged propagator (the term in the large brackets) for a studied confining domain (*36*).

The formula [15] for short gradient pulses is a keystone for many experimental and theoretical studies [see reviews (*1*, *37–39*) and references therein]. This is a broadly accepted way of thinking about restricted diffusion in NMR. If this relation was always applicable, further discussions in this article would not be necessary. However, the description by short gradient pulses is approximate. The implicit hypothesis is that the gradient pulses are so narrow in time that diffusion of particles during these pulses (time δ) can be neglected. This hypothesis *may* or *may not* be satisfied. In practice, this so-called narrow-pulse approximation is often applicable for liquids and sometimes for gases. As a counter example, DWI of the lungs with hyperpolarized helium-3 gas, which is usually performed with gradients of intensity $g \sim 1$ mT m^{-1} and duration $\delta \sim 1$ ms (*40–42*) is considered. For the diffusion coefficient D of helium around 1 cm^{2}s^{-1}, the phase shift uncertainty $\gamma g \delta \sqrt{2D\delta}$ is in the order of 0.1 (with $\gamma \simeq 2 \times 10^8$ rad $T^{-1}s^{-1}$ for helium-3 nuclei). Under these conditions, the narrow-pulse approximation is not applicable.

A number of theoretical, numerical and experimental studies concerned the applicability of the narrow-pulse approximation (*43–47*). The revision of the related literature does not respond to the aims of this article. Whether this approximation is applicable or not, the concept of using two very short gradient pulses remains restrictive from another point of view. In the narrow-pulse approximation, one encodes only the starting and arrival points, throwing away the full trajectory of a particle. In contrast, the application of an inhomogeneous magnetic field continuously, during the whole experiment, allows one to encode the full trajectory, providing a priori richer information about restricted diffusion. Moreover, one has a freedom to vary the intensity of the magnetic field in time. Figuratively speaking, the difference between the narrow-pulse approximation and a continuous encoding is similar to that between taking two snapshots and filming a whole movie. The fact that the analysis of continuously encoded trajectories is not simple should not be the reason for rejecting this research modality which is potentially richer. In Section III, it is shown that the mathematical basis for studying continuously encoded trajectories is in fact as well developed as that of the narrow-pulse approximation.

Notion of Eigenfunction

The dynamics of particles is often represented by a linear operator. For instance, diffusive dynamics is represented by the Laplace operator or, more generally, by an elliptic second-order differential operator. Among a variety of functions on which a linear operator can act, the eigenfunctions are those which are invariant under the action of the operator, up to multiplicative factors. Eigenfunctions are the "elementary blocks" for describing the action of an operator in an appropriate functional space. The Laplace operator in a bounded domain Ω with Dirichlet, Neumann or Robin boundary condition is thoroughly investigated in mathematics (*48*, *49*). It is well known that this operator has a discrete spectrum and an infinite set of eigenfunctions $u_m(\mathbf{r})$ (enumerated by $m = 0,1,2,\ldots$)

$$\begin{aligned} &\Delta u_m(\mathbf{r}) + \lambda_m u_m(\mathbf{r}) = 0 \quad (\mathbf{r} \in \Omega), \\ &D\frac{\partial}{\partial n} u_m(\mathbf{r}) + K u_m(\mathbf{r}) = 0 \quad (\mathbf{r} \in \partial\Omega), \end{aligned} \qquad [16]$$

where D and K are the macroscopic transport coefficients (Sections "Microscopic Dynamics" and "Boundary Condition"). The corresponding eigenvalues λ_m are positive. It is convenient to enumerate the eigenvalues in an ascending order: $0 \le \lambda_0 \le \lambda_1 \le \lambda_2 \le \ldots$, increasing up to infinity. The number of eigenvalues λ_m smaller than $\lambda > 0$ obeys the Weyl asymptotic law (*50*)

$$\#\{m : \lambda_m < \lambda\} \propto \lambda^{d/2} \quad (\lambda \to \infty). \qquad [17]$$

The eigenfunctions $u_m(\mathbf{r})$ are orthogonal and conveniently normalized

$$\int\limits_{\Omega} d\mathbf{r}\, u_m(\mathbf{r}) u^*_{m'}(\mathbf{r}) = \delta_{m,m'}, \qquad [18]$$

where the asterisk denotes a complex conjugate, and $\delta_{m,m'}$ is the Kronecker symbol ($\delta_{m,m'} = 1$ for $m = m'$, and 0 otherwise). This normalization implies that the eigenfunctions are in units of m$^{-d/2}$, while the eigenvalues are in units of m^{-2}, independently of the dimension d.

The Laplace operator eigenfunctions satisfy the completeness relation,

$$\sum_m u_m(\mathbf{r}) u_m^*(\mathbf{r}') = \delta(\mathbf{r} - \mathbf{r}'),$$

which allows one to decompose any square integrable function $\upsilon(\mathbf{r})$ on the complete basis of eigenfunctions. For this purpose, one multiplies the above relation by $\upsilon(\mathbf{r}')$ and integrates over Ω:

$$\sum_m u_m(\mathbf{r}) \int_\Omega d\mathbf{r}'\, u_m^*(\mathbf{r}')\, \upsilon(\mathbf{r}') = \int_\Omega d\mathbf{r}'\, \delta(\mathbf{r} - \mathbf{r}')\, \upsilon(\mathbf{r}') = \upsilon(\mathbf{r}).$$

In the field of wave propagation, Laplacian eigenfunctions have a natural interpretation as vibration modes. Any vibration mode can be individually excited at the corresponding (eigen) frequency. For diffusion, a geometrical interpretation is less apparent. For instance, the diffusive propagator can be decomposed into a sum of eigenfunctions which are "mixed" with different time-dependent weights:

$$G_t(\mathbf{r}, \mathbf{r}') = \sum_m u_m^*(\mathbf{r}) u_m(\mathbf{r}') e^{-D\lambda_m t}. \qquad [19]$$

It is easy to check that the right-hand side of this relation satisfies Eqs. [3,4,6] that uniquely determines the diffusive propagator $G_t(\mathbf{r},\mathbf{r}')$. Each eigenvalue sets a "lifetime", $(D\lambda_m)^{-1}$, of the corresponding eigenstate.

The information hidden in eigenfunctions is very rich but difficult to extract in an experiment. In contrast to wave equation, there is no "resonance frequency" at which a particular eigenmode can be excited. In addition, the preparation of a diffusive system in a particular eigenstate is problematic. Distinguishing contributions from individual eigenmodes is therefore challenging. Nonetheless, Song and coworkers reported an experimental demonstration of the excitation and detection of a wide range of eigenmodes in porous media by exploring the inhomogeneous internal magnetic field in the pore space (*51–53*).

What can the shape of an eigenmode tell us? We start with the ground eigenmode u_0 which, according to Perron-Frobenius theorem, is the unique eigenmode which is positive whole domain. For a purely reflecting boundary, the ground eigenmode u_0 is a constant which is a truly equilibrium state of a system. In this case, the system tends to diminish all fluxes and reaches its equilibrium when all the fluxes are zero (a constant density). The associated (lowest) eigenvalue λ_0 is zero that corresponds to an infinite lifetime of the equilibrium eigenmode.

When a boundary is (partially) absorbing, all the eigenvalues are strictly positive, and the equilibrium state is zero concentration (no particle left). In the long-time regime, the ground eigenmode u_0 provides the main contribution to Eq. [19], while the other eigenmodes are exponentially small in comparison with u_0. Although the ground eigenmode is not a truly equilibrium state, it plays a role of a steady state. The "survived" particles are distributed in a diffusion-confining domain to minimize their losses, i.e., to be as far from the absorbing boundary as possible (Fig. 3). The ground eigenmode reaches its maximum in the "center" of the domain (this is not necessarily a barycenter or another "geometrical" center, but a "diffusion center").

The other eigenmodes $u_m(\mathbf{r})$ are orthogonal to u_0. Since u_0 is positive, the $u_m(\mathbf{r})$ must change their sign over the domain. In other words, the eigenfunctions oscillate, although these "oscillations" are adapted to the shape of the domain and are not necessarily periodic (Fig. 3). The square root of an eigenvalue, $\sqrt{\lambda_m}$, determines a spatial frequency (the inverse of a wavelength) of the associate eigenmode. An analogy with sine and cosine functions (which are the Laplacian eigenmodes on the interval) is instructive.

How can one interpret the shape of an oscillating eigenfunction? Its negative values prohibit thinking of an eigenfunction as a density, but one can consider it as an excess/deficiency distribution. If a system was initially prepared in such an eigenstate, $c(\mathbf{r}, 0) = u_m(\mathbf{r})$, the evolution in time would not change the initial spatial profile but would only attenuate it by the corresponding exponential factor: $c(\mathbf{r}, t) = e^{-D\lambda_m t} u_m(\mathbf{r})$. The shape of an eigenfunction visually shows diffusive exchange areas of a confining domain. The particles diffuse from maxima to minima of an eigenfunction to level off any excess or deficiency. This interpretation allows one to use Laplacian eigenfunctions to detect exchange areas, while the associated eigenvalues give the characteristic time and length scales of an exchange process. Although separating these contributions is difficult in an experiment, the related theoretical analysis is expected to be instructive, especially for complex geometries.

Asymptotic Behavior

Most theoretical results on restricted diffusion are somehow related to the asymptotic behavior of the diffusive propagator $G_t(\mathbf{r},\mathbf{r}')$. These asymptotic results are often expressed through explicit analytical formulas that makes them particularly useful in practice (e.g., for fitting the macroscopic signal or for

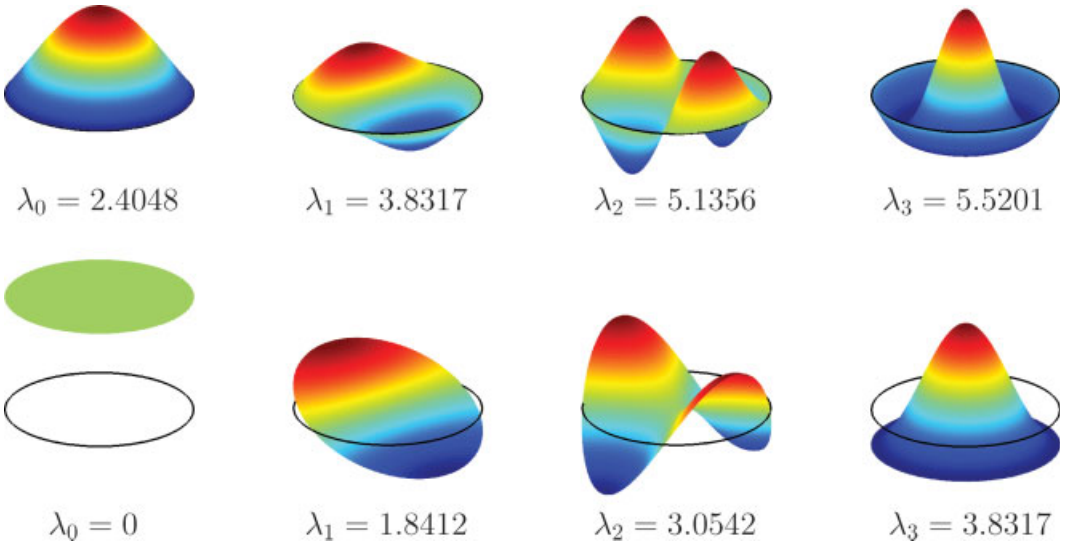

Figure 3 First four eigenfunctions of the Laplace operator in the unit disk with Dirichlet (top) and Neumann (bottom) boundary conditions (the associated eigenvalues are shown). Apart from the positive ground eigenmode (on the left), the other eigenfunctions "oscillate" that can be interpreted as diffusive exchanges between their maxima and minima. The larger the eigenvalue λ_m (the smaller the corresponding wavelength), the higher is the oscillation spatial frequency $\sqrt{\lambda_m}$ but the shorter is the "lifetime" $(D\lambda_m)^{-1}$ of the eigenmode. [Color figure can be viewed in the online issue, which is available at www.interscience.wiley.com.]

extracting information on the geometry of a confining medium).

Long-Time Regime. The long-time regime, for which the diffusion length $\sqrt{DT}$ is much longer than the size L of a confining domain, is rather simple for investigation. The contributions of eigenmodes in Eq. [19] progressively vanish as time goes on so that the ground eigenmode with the lowest eigenvalue λ_0 becomes the only significant contribution when

$$T \gg (D\lambda_1)^{-1} \geq (D\lambda_2)^{-1} \geq \dots$$

The eigenvalue λ_1 sets the lower time bound $(D\lambda_1)^{-1}$ for the long-time regime. Since λ_1 is presumably in the order of L^{-2}, the condition $\sqrt{DT} \gg L$ is enough for practical purposes.

The lowest eigenvalue λ_0 determines the main transport characteristics of a system, e.g., the reaction rate of a diffusion-mediated reactor (*54–56*) and surface relaxation times in NMR (*57*). The distinction between purely and partially reflecting boundaries is pronounced in the long-time regime. The propagator either approaches a constant (pure reflections) or exponentially decays (partial reflections). Although too idealized from a physical point of view, the concept of a purely reflecting boundary is justified if the lifetime $(D\lambda_0)^{-1}$ of the ground eigenmode is much longer than the observation time. In this situation, many results can be simplified (see later).

It is worth noting a significant distinction between unrestricted diffusion and restricted diffusion in a bounded domain. For fixed positions $\mathbf{r}$ and $\mathbf{r}'$, the exponential function in Eq. [2] approaches 1 as t going to infinity so that the propagator for free diffusion in the whole space shows a power-law decay:

$$G_t(\mathbf{r},\mathbf{r}') \simeq \frac{1}{(4\pi Dt)^{d/2}} \quad (t \to \infty),$$

in sharp contrast to an exponential approach to a constant for a bounded domain with Neumann boundary condition

$$G_t(\mathbf{r},\mathbf{r}') \simeq \frac{1}{V} + u_1^*(\mathbf{r})u_1(\mathbf{r}')e^{-D\lambda_1 t} \quad (t \to \infty).$$

At the same time, both a relaxing boundary of a bounded domain and relaxing sinks in an unbounded medium lead to an exponential decay of the signal.

Short-Time Regime. The short-time regime is a different story. On one hand, the smaller the time t, the larger is the number of contributing eigenfunctions in Eq. [19]. In the limit of t going to 0, the diffusive propagator approaches a Dirac distribution that makes a numerical computation challenging.

One can appreciate this difficulty by computing numerically the simplest propagator for restricted diffusion on the unit interval for very small times t:

$$G_t(x,x') = 1 + 2\sum_{m=1}^{\infty} \cos(\pi m x)\cos(\pi m x') e^{-D\pi^2 m^2 t}. \quad [20]$$

This formula comes from the general spectral decomposition [19] in which $\cos(\pi m x)$ and $\pi^2 m^2$ are the eigenfunctions and eigenvalues of the Laplace operator on the unit interval with reflecting endpoints.

On the other hand, the smaller the time, the closer is the $G_t(\mathbf{r}, \mathbf{r}')$ to the free diffusive propagator which is known explicitly. In fact, the particles just do not have enough time to explore the domain and to "feel" the presence of restricting boundaries. When points $\mathbf{r}$ and $\mathbf{r}'$ do not belong to the boundary, one can use the short-time approximation:

$$\sum_m u_m^*(\mathbf{r}) u_m(\mathbf{r}') e^{-D\lambda_m t} \simeq \frac{1}{(4\pi D t)^{d/2}} \exp\left[-\frac{(\mathbf{r}-\mathbf{r}')^2}{4Dt}\right] \quad (t \to 0). \quad [21]$$

This simple formula allows one to derive a number of asymptotic results.

Series with Eigenvalues. As discussed in Section III, one often needs to investigate the short-time asymptotic behavior of series involving the Laplacian eigenvalues:

$$F(t) = \sum_m F_m e^{-D\lambda_m t}, \quad [22]$$

with some coefficients F_m.

A general but rough estimation of the series relies on the fact that e^{-x} is close to 1 for small x and to 0 for large x. When t is small enough, there are many eigenvalues for which $D\lambda_m t \ll 1$. At the same time, there are always an infinity of eigenvalues for which $D\lambda_m t \gg 1$ (because the sequence of λ_m increases toward infinity). The time t sets a border index M between these two cases: $D\lambda_M t \sim 1$. The Weyl's law [17] relates λ_M to M as $M \propto \lambda_M^{d/2} \propto t^{-d/2}$. In a first approximation, $e^{-D\lambda_m t}$ can be replaced by 1 for $m \leq M$, and by 0 otherwise. This crude approximation yields

$$F(t) \simeq \sum_{m=1}^{M} F_m \propto \int_1^{t^{-d/2}} F_m dm.$$

For example, if $F_m \propto m^{\alpha-1}$, one gets

$$F(t) \propto t^{-\alpha d/2} \quad (t \to 0).$$

In the case $F_m = 1$ ($\alpha = 1$), one deduces the short-time asymptotic behavior of the spectral function $\eta(t)$ or, equivalently, of the averaged probability of return to the origin:

$$\eta(t) \equiv \sum_m e^{-D\lambda_m t} = \int_\Omega d\mathbf{r}\, G_t(\mathbf{r},\mathbf{r}) \propto t^{-d/2} \quad (t \to 0).$$

This rough estimation approach yields in general correct asymptotic behavior, but it fails to give proportionality factors or correction terms.

Laplace Transform and Summation Techniques. The knowledge of the asymptotic behavior alone is insufficient for an accurate comparison between theory and experiment. For instance, the determination of the surface-to-volume ratio of a diffusion-confining domain at short times is based on the $t^{3/2}$ correction term and its coefficient, as explained in section "Short-Time Diffusion Regime: Corrections".

A more accurate analysis relies on the Laplace transform $\mathcal{L}$ of the series in Eq. [22]

$$\hat{F}(s) \equiv \mathcal{L}[F(t)](s) \equiv \int_0^\infty dt\, e^{-ts} F(t) = \sum_m \frac{F_m}{s + D\lambda_m}$$

If the coefficients F_m are rational functions of λ_m, $\hat{F}(s)$ can be reduced to an algebraic expression which contains the Laplace transform $\hat{\eta}(s)$ of the spectral function $\eta(t)$ and its derivatives (*1*)

$$\hat{\eta}(s) \equiv \mathcal{L}[\eta(t)](s) = \sum_m \frac{1}{s + D\lambda_m}. \quad [23]$$

As an arbitrary example, let us take $F_m = 1/\lambda_m$, for which

$$\hat{F}(s) = \sum_m \frac{1}{\lambda_m(s + D\lambda_m)} = \sum_m \frac{1}{s}\left(\frac{1}{\lambda_m} - \frac{D}{s + D\lambda_m}\right) = D\frac{\hat{\eta}(0) - \hat{\eta}(s)}{s}.$$

A series expansion of $\hat{F}(s)$ in powers of $1/s$ as s going to infinity allows one to reconstruct the asymptotic behavior of $F(t)$ as t going to 0 by using the relation

$$\mathcal{L}[t^{\beta-1}](s) = \int_0^\infty dt\, t^{\beta-1} e^{-ts} = s^{-\beta} \int_0^\infty d\tilde{t}\, \tilde{t}^{\beta-1} e^{-\tilde{t}}$$
$$= s^{-\beta}\Gamma(\beta),$$

$\Gamma(\beta)$ being the Gamma function.

For simple shapes such as interval, disk, and sphere, the eigenvalues λ_m are known to be the squared zeros α_m of some explicit functions (e.g., Bessel functions for the disk) (*58*, *59*). In this case, the function $\hat{\eta}(s)$ can be calculated explicitly (*60*) that opens a possibility for the investigation of various spectral series. For instance, the constants $\zeta_{3/2}, \zeta_{-1}, \zeta_{-2}$ that determine the geometry dependence of the macroscopic signal in the short-time and long-time regimes (see sections "Short-Time Diffusion Regime: Corrections" and "Long-Time Diffusion Regime"), were found in this way (*1*).

In this section, the question of convergence is not addressed. In practice, the convergence of spectral series can be improved by differentiation or integration. For instance, the spectral series of the derivative of $\hat{F}(s)$, which represents the Laplace transform of $-tF(t)$, converges better than that of $\hat{F}(s)$:

$$-\hat{F}'(s) = \mathcal{L}[tF(t)](s) = \sum_m \frac{F_m}{(s + D\lambda_m)^2}.$$

When the asymptotic behavior of $\hat{F}'(s)$ is found, it is easy to deduce that of $F(t)$. Similarly, the integration of $F(t)$ improves the convergence of the series in Eq. [22] due to an additional factor λ_m^{-1}. A more detailed discussion of these issues goes beyond the scope of this work.

III. THEORETICAL ADVANCES

In Part 1, a matrix formalism is presented as an efficient numerical tool for studying restricted diffusion in NMR. The Bloch-Torrey equation that describes the evolution of the magnetization in time is projected onto the Laplacian eigenfunctions. In this basis, the magnetization is represented by an infinite-dimensional vector which is composed of unknown time-dependent coefficients. The use of the Laplacian eigenfuctions reduces the Bloch-Torrey equation, a PDE in space and time, to a linear system of first-order differential equations in time. A solution of this system is then written in a compact matrix form. The two governing infinite-dimensional matrices Λ and $\mathcal{B}$ represent the Laplace operator and the applied magnetic field $B(\mathbf{r})$, respectively, in the Laplacian eigenbasis:

$$\Lambda_{m,m'} = \int_\Omega d\mathbf{r}\; u_m^*(\mathbf{r})(-L^2\Delta)u_{m'}(\mathbf{r}) = \delta_{m,m'}\lambda_m L^2,$$
$$\mathcal{B}_{m,m'} = \int_\Omega d\mathbf{r}\; u_m^*(\mathbf{r})\, B(\mathbf{r}) u_{m'}(\mathbf{r}), \qquad [24]$$

where the factor L^2 is introduced for getting dimensionless matrix elements. Once these matrices are found for a given diffusion-confining domain, further computation is easy, rapid, and very accurate. Explicit formulas for the matrices Λ and $\mathcal{B}$ for simple shapes such as interval, disk, and sphere are given in (*1*, *61*).

At the same time, a theoretical analysis relying on the above matrix formalism faces considerable difficulties because the governing matrices $\mathcal{B}$ and Λ do not commute. Another mathematical approach is required for the investigation of the macroscopic signal. In this section, we present such an approach and explain how the moments of a random phase shift can be expressed in terms of the matrices Λ and $\mathcal{B}$. This article focuses on the zeroth, first, and second moments which provide the major contribution to the macroscopic signal. The short-time and long-time regimes are discussed in detail. The obtained results are broadly used in practice to interpret experimentally measured signals and to extract information on the geometry of a diffusion-confining medium.

Formal Probabilistic Description

In most diffusion-encoding NMR experiments, the temporal and spatial variations of an applied magnetic field are factored:

$$B(\mathbf{r},t) = \beta f(t/T) B(\mathbf{r}),$$

where β is the dimensional intensity of the magnetic field (in Tesla), $f(t)$ is the effective dimensionless temporal profile, and $B(\mathbf{r})$ is the dimensionless spatial profile. The temporal profile $f(t)$ is often chosen to satisfy the rephasing condition

$$\int_0^T dt\, f(t/T) = 0. \qquad [25]$$

A physical meaning of the rephasing condition is simple. If nuclei were immobile, their total phase shift would be strictly zero because an initial dephasing would be completely compensated by a later rephasing. For such immobile nuclei, the macroscopic signal at observation time T would be 1. When

nuclei diffuse, the rephasing is not complete, and the macroscopic signal decreases. This experimentally measurable attenuation characterizes diffusive motion. In practice, a temporal profile is usually composed of two rectangular or trapezoidal pulses of opposite polarities (Fig. 4). The profile $f(t)$ may also incorporate the inversion effect of the 180° rf pulse. The standard choice for a spatial profile $B(\mathbf{r})$ is a linear gradient in a given direction $\mathbf{e}$: $B(\mathbf{r}) = (\mathbf{e} \cdot \mathbf{r})/L$.

The definition [9] of the phase shift can be written as follows

$$\varphi = \underbrace{\gamma\beta T}_{q}\,\phi, \quad \phi = \int_0^1 dt\, f(t) B(X_t), \qquad [26]$$

where we changed the time variable and rescaled the reflected Brownian motion: $X_t = \mathbf{r}(tT)$. From now on, t is the dimensionless time variable varying from 0 to 1. In Eq. [26], ϕ is a new random variable representing a phase shift, while the factor $q = \gamma\beta T$ is the dimensionless intensity. For a linear gradient of intensity g, one has $\beta = gL$, and

$$q = \gamma g T L$$

is the ratio between the size L of a diffusion-confining domain and the dephasing length $(\gamma g T)^{-1}$ which is induced by the applied magnetic field gradient.

In mathematical terms, the problem consists in finding the probability density $P(\phi)$ of the random variable ϕ for a given magnetic field [functions $f(t)$ and $B(\mathbf{r})$] and a given confining domain Ω. This problem can formally be solved by writing the definition of the characteristic function:

$$\mathbb{E}\{e^{iq\phi}\} = \int_{-\infty}^{\infty} d\phi\, e^{iq\phi} P(\phi).$$

According to Eq. [10], $\mathbb{E}\{e^{iq\phi}\}$ is the macroscopic signal, for which an explicit matrix formula was derived in Part 1. For instance, for a time-independent magnetic field, with $f(t) = 1$, Eq. [I.29] from (2) states that

$$\mathrm{E}\{e^{iq\phi}\} = (U e^{-(p\Lambda + iqB)} \tilde{U}), \qquad [27]$$

where

$$p = DT/L^2$$

is the dimensionless diffusion coefficient that characterizes how far the nuclei diffuse on average during the time T. This is the squared ratio between the diffusion length $\sqrt{DT}$ and the size L of a diffusion-confining domain.

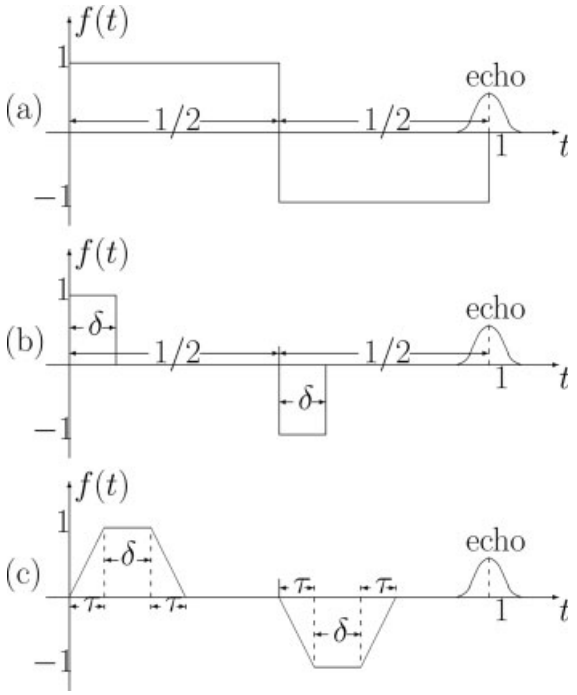

Figure 4 Examples of effective temporal profiles: (a) steady, (b) Stejskal-Tanner rectangular, (c) trapezoidal. The 180° rf pulse is taken into account by the opposite sign of the second gradient pulse. All three examples satisfy the rephasing condition [25]. It is reminded that time is dimensionless here so that the observation time T (formation of an echo) corresponds to $t = 1$. The duration δ of two gradient pulses and the ramp time τ are also dimensionless.

The infinite-dimensional vectors U and $\tilde{U}$ in Eq. [27] represent an initial density $\rho(\mathbf{r})$ and a sampling or pickup function $\tilde{\rho}(\mathbf{r})$ in the Laplacian eigenbasis:

$$\begin{aligned} U_m &= V^{1/2} \int_\Omega d\mathbf{r}\, u_m^*(\mathbf{r}) \rho(\mathbf{r}), \\ \tilde{U}_m &= V^{-1/2} \int_\Omega d\mathbf{r}\, u_m(\mathbf{r}) \tilde{\rho}(\mathbf{r}) \end{aligned} \qquad [28]$$

(the prefactors $V^{1/2}$ and $V^{-1/2}$ are introduced for getting dimensionless quantities). If the density of non-polarized spins at the beginning of the experiment is uniform and if the exciting 90° rf pulse is spatially homogeneous, the initial magnetization is proportional to the initial density $\rho(\mathbf{r})$, and thus uniform: $\rho(\mathbf{r}) = 1/V$. In addition, the sampling or pickup function $\tilde{\rho}(\mathbf{r})$ is often uniform throughout the sample: $\tilde{\rho}(\mathbf{r}) = 1$. In this case, one gets

$$U_m^* = \tilde{U}_m = V^{-1/2} \int_\Omega d\mathbf{r}\, u_m(\mathbf{r}). \qquad [29]$$

In a general situation of a given temporal profile $f(t)$, Eq. [27] can be extended by dividing the time interval in small subintervals $[t_k, t_{k+1})$ ($k = 0,\ldots,K$, with $t_0 = 0$ and $t_{K+1} = 1$) and approximating $f(t)$ by a piecewise constant function: $f(t) = f_k$ for $t \in [t_k, t_{k+1})$. As shown in Part 1, the characteristic function is

$$\mathbb{E}\{e^{iq\phi}\} \simeq (U \prod_{k=0}^{K} e^{-(p\Lambda + iqf_k\mathcal{B})(t_{k+1}-t_k)}\tilde{U}).$$

The matrices Λ and $\mathcal{B}$ and the vectors U and $\tilde{U}$ fully determine the characteristic function $\mathbb{E}\{e^{iq\phi}\}$ and, through the inverse Fourier transform, the probability density $P(\phi)$. Formally, the problem of finding the random phase shift ϕ (or φ) is therefore solved. Moreover, one can expand the characteristic function into a Taylor series in powers of q in order to obtain the moments $\mathbb{E}\{\phi^n\}$:

$$\mathbb{E}\{\phi^n\} = i^{-n} \lim_{q\to 0}\left(\frac{\partial^n}{\partial q^n}\mathbb{E}\{e^{iq\phi}\}\right).$$

However, the matrix structure of Eq. [27] makes further theoretical analysis challenging. In particular, the differentiation of matrix exponentials is difficult, both analytically and numerically. It is thus important to derive an alternative expression for the moments by considering the random phase ϕ as a functional [26] of reflected Brownian motion.

Zeroth Moment

The analysis is started by considering the zeroth moment of the random phase φ: $\mathbb{E}\{\phi^0\} = \mathbb{E}\{1\}$. At first thought, it may sound nonsense to take an average of a constant. One should not forget, however that this average includes implicitly restrictions on the trajectories of reflected Brownian motion in a diffusion-confining domain. Moreover, the starting and arrival points may be chosen specifically that would also influence the results. The following computation of the zeroth moment illustrates many concepts of the probabilistic description. This computation corresponds to an experiment, in which diffusion weighting is realized through surface relaxation (without any applied gradient).

What does the expectation $\mathbb{E}\{1\}$ mean? It is reminded that particles started with a given initial density $\rho(\mathbf{r})$, i.e., the starting point $\mathbf{r}_0$ is picked up at random, with the probability $\rho(\mathbf{r}_0)d\mathbf{r}_0$. When a nucleus started from $\mathbf{r}_0$, its probability for arriving in a vicinity $d\mathbf{r}$ of a point $\mathbf{r}$ at time T is $G_1(\mathbf{r}_0, \mathbf{r})d\mathbf{r}$ (it is reminded that the observation time T corresponds to dimensionless time $t = 1$). The contribution of such Brownian trajectories is weighted with a sampling function $\tilde{\rho}(\mathbf{r})$ (Fig. 5). The average over all starting and arrival points $\mathbf{r}_0$ and $\mathbf{r}$ reads as follows:

$$\mathbb{E}\{1\} = \int_\Omega d\mathbf{r}_0\rho(\mathbf{r}_0)\int_\Omega d\mathbf{r}\; G_1(\mathbf{r}_0,\mathbf{r})\tilde{\rho}(\mathbf{r}).$$

The eigenmode expansion [19] for the diffusive propagator $G_1(\mathbf{r}_0,\mathbf{r})$ allows one to separate two integrals:

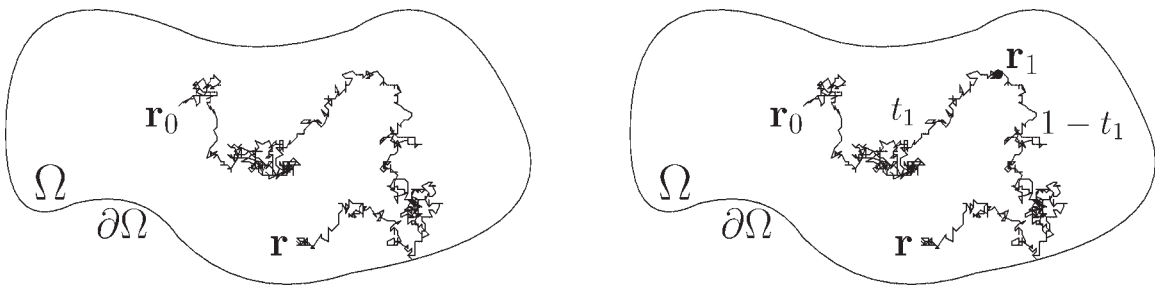

Figure 5 Probabilistic computation of the zeroth (left) and first (right) moments. In both cases, a set of Brownian trajectories is considered which started from a randomly chosen point $\mathbf{r}_0$ and arrived into a small vicinity of a random point $\mathbf{r}$. The zeroth moment $\mathbb{E}\{1\}$ represents a "fraction" of the nuclei (or trajectories) which survived up to the observation time. For the first moment $\mathbb{E}\{\phi\}$, an intermediate position $\mathbf{r}_1$ is encoded by an infinitely short magnetic field pulse $\delta(t - t_1)B(\mathbf{r}_1)$. Two diffusive propagators, $G_{t_1}(\mathbf{r}_0,\mathbf{r}_1)$ and $G_{1-t_1}(\mathbf{r}_1,\mathbf{r})$, describe the motion of nuclei between $\mathbf{r}_0$ and $\mathbf{r}_1$, and that between $\mathbf{r}_1$ and $\mathbf{r}$, respectively. Similarly, two intermediate positions $\mathbf{r}_1$ and $\mathbf{r}_2$ are encoded by two magnetic field pulses for the second moment $\mathbb{E}\{\phi^2/2\}$, and so on.

$$\mathbb{E}\{1\} = \sum_m \left[\int_\Omega d\mathbf{r}_0 \rho(\mathbf{r}_0) u_m^*(\mathbf{r}_0)\right] e^{-D\lambda_m T} \times \left[\int_\Omega d\mathbf{r}\, u_m(\mathbf{r})\tilde{\rho}(\mathbf{r})\right].$$

These two integrals give the elements of the vectors U and $\tilde{U}$ that is a spectral representation of the initial density $\rho(\mathbf{r}_0)$ and of the sampling function $\tilde{\rho}(\mathbf{r})$ in the Laplacian eigenbasis. If $e^{-D\lambda_m T}$ is considered as a diagonal element of the matrix $e^{-p\Lambda}$, the above sum becomes a matrix product

$$\mathbb{E}\{1\} = (U\, e^{-p\Lambda}\tilde{U}). \qquad [30]$$

Although this relation could be directly deduced from Eq. [27] by putting $q = 0$, it is prefered to give this probabilistic "derivation" that will serve as an illustration for other moments.

When the initial density and the sampling function are uniform, Eq. [29] allows one to retrieve the classical spectral expansion by Brownstein and Tarr (*57*):

$$\mathbb{E}\{1\} = \sum_m \frac{1}{V}\left|\int_\Omega d\mathbf{r}\, u_m(\mathbf{r})\right|^2 e^{-D\lambda_m T}. \qquad [31]$$

If there is no magnetic field gradient, the macroscopic signal is simply equal to the zeroth moment: $E = \mathbb{E}\{1\}$.

For a purely reflecting boundary (when the dimensionless surface relaxavity $h = KL/D$ is 0), the ground eigenfunction u_0 is constant. Since the other eigenfunctions are orthogonal to u_0, the only nonzero term in the above sum comes from the ground state $m = 0$ for which $\lambda_0 = 0$ so that $E = \mathbb{E}\{1\} = 1$. Naturally, if there is no relaxation mechanism at all (neither surface or bulk relaxation nor gradient encoding), the macroscopic signal is constant.

For a partially absorbing boundary ($h > 0$), all the eigenvalues are strictly positive that yields a multiexponential decrease of the macroscopic signal in time. Given the spectral expansion [19] of a propagator, a multiexponential behavior is a natural feature of restricted diffusion [e.g., its consequences for a CPMG sequence is discussed in (*62*)]. Deviations from this typical behavior are in general caused either by too many contributing eigenmodes in the short-time regime (e.g., asymptotic behavior [21] or power-law decays) or by too few contributing eigenmodes in the long-time regime. In the latter case, the major contribution comes from the lowest eigenvalue λ_0 for which the exponential factor in Eq. [31] is less attenuated:

$$E \simeq U_0^2 e^{-D\lambda_0 T}.$$

If the surface relaxation is weak (small h), a perturbative analysis shows that the lowest eigenvalue λ_0 is proportional to h: $\lambda_0 \simeq h(S/V)/L$, where S is the total surface area of a diffusion-confining medium (*63*). In addition, $U_0^2 \simeq 1$ (for small h) that yields

$$E \simeq \exp[-K(S/V)T],$$

where K is the surface relaxivity (section "Boundary Condition"). This fast-diffusion regime allows one to determine the surface-to-volume ratio S/V of a confining domain (*57*). This simple result is often used to characterize porous media. If a porous medium is considered as an ensemble of disconnected "pores," the macroscopic signal is the sum of signals from individual pores. It can also be written as the Laplace transform of the distribution of the surface-to-volume ratios:

$$E \simeq \sum_{\text{pore } i} I_i \exp[-K(S/V)_i T] = \int_0^\infty ds\, e^{-sT}\left[\sum_{\text{pore } i} I_i \delta(s - K(S/V)_i)\right],$$

where I_i is the relative signal intensity from a pore i. Since the surface-to-volume ratio of a sphere-like pore is related to its size, one can extract the pore size distribution (*64*, *65*).

First Moment

When a diffusion-encoding gradient is applied, the first and higher-order moments have to be analyzed. Since the magnetic field varies both in time and space, it is convenient (and even necessary) to separate temporal and spatial variations. For this purpose, a magnetic field is formally written as follows:

$$\beta f(t) B(\mathbf{r}) = \beta \int_0^1 dt_1 f(t_1)\,[\delta(t - t_1) B(\mathbf{r})].$$

To calculate the first moment, one can find the phase shift due to an infinitely short magnetic field pulse $\beta\delta(t - t_1)B(\mathbf{r})$ and then "sum up" all contributions with weights $f(t_1)$:

$$\mathbb{E}\{\phi\} = \int_0^1 dt_1 f(t_1)\, \mathbb{E}\{B(X_{t_1})\}. \qquad [32]$$

This relation simply reflects the fact that expectation is a linear operation. The one-point correlation function $\mathbb{E}\{B(X_{t_1})\}$ can be interpreted as the average phase shift acquired due to an infinitely short magnetic field pulse $\delta(t - t_1)B(\mathbf{r})$. The dynamics of the nuclei diffusing without a magnetic field (except for the moment t_1) is characterized by a diffusive propagator. As Brownian motion is a Markov process (with no memory), one can "split" a random trajectory of a nucleus into two independent parts, before and after time t_1 (Fig. 5). In other words,

- at time $t = 0$, one chooses a random starting point $\mathbf{r}_0$ with the initial density $\rho(\mathbf{r}_0)$ (or the starting probability $\rho(\mathbf{r}_0)d\mathbf{r}_0$);
- during time t_1, a nucleus diffuses from $\mathbf{r}_0$ into a small vicinity $d\mathbf{r}_1$ of a random point $\mathbf{r}_1$ with probability $G_{t_1}(\mathbf{r}_0,\mathbf{r}_1)d\mathbf{r}_1$;
- the nucleus acquires the phase $B(\mathbf{r}_1)$ at point $\mathbf{r}_1$ due to the infinitely short magnetic field pulse;
- during the remaining time $1 - t_1$, the nucleus diffuses from $\mathbf{r}_1$ into a small vicinity $d\mathbf{r}$ of a random point $\mathbf{r}$ with probability $G_{1-t_1}(\mathbf{r}_1,\mathbf{r})d\mathbf{r}$;
- its contribution is weighted by a pickup or sampling function $\tilde{\rho}(\mathbf{r})$.

Here, the propagators $G_{t_1}(\mathbf{r}_0,\mathbf{r}_1)$ and $G_{1-t_1}(\mathbf{r}_1,\mathbf{r})$ already represent the averages over all Brownian trajectories between $\mathbf{r}_0$ and $\mathbf{r}_1$ during time t_1 and between $\mathbf{r}_1$ and $\mathbf{r}$ during time $1 - t_1$. The average phase acquired due to the infinitely short magnetic field pulse is then obtained by averaging over the points $\mathbf{r}_0$, $\mathbf{r}_1$, and $\mathbf{r}$:

$$\mathbb{E}\{B(X_{t_1})\} = \int_\Omega \underbrace{d\mathbf{r}_0\, \rho(\mathbf{r}_0)}_{\substack{\text{choosing}\\ \text{starting}\\ \text{point } \mathbf{r}_0}} \int_\Omega \underbrace{d\mathbf{r}_1\, G_{t_1}(\mathbf{r}_0,\mathbf{r}_1)}_{\substack{\text{diffusing}\\ \text{from } \mathbf{r}_0 \text{ to}\\ \mathbf{r}_1 \text{ at time } t_1}} \underbrace{B(\mathbf{r}_1)}_{\substack{\text{acquiring}\\ \text{the phase}\\ \text{at } \mathbf{r}_1}} \int_\Omega \underbrace{d\mathbf{r}\, G_{1-t_1}(\mathbf{r}_1,\mathbf{r})}_{\substack{\text{diffusing}\\ \text{from } \mathbf{r}_1 \text{ to } \mathbf{r}\\ \text{at time } 1-t_1}} \underbrace{\tilde{\rho}(\mathbf{r})}_{\substack{\text{sampling}\\ \text{arrival}\\ \text{points } \mathbf{r}}}$$

averaging over starting points; averaging over encoded points; averaging over arrival points

$$\mathbb{E}\{B(X_{t_1})\} = \sum_{m_1=0}^{\infty} \sum_{m_2=0}^{\infty} U_{m_1}\, e^{-D\lambda_{m_1}Tt_1}\, \mathcal{B}_{m_1,m_2}\, e^{-D\lambda_{m_2}T(1-t_1)}\, \tilde{U}_{m_2}$$

Using the eigenmode expansion [19] for a diffusive propagator, one gets the above spectral decomposition. Representing the eigenvalues λ_m by the diagonal elements of the matrix Λ, one can write the above relation in a compact matrix form

$$\mathbb{E}\{B(X_{t_1})\} = (U\, e^{-p\Lambda t_1}\, \mathcal{B}\, e^{-p\Lambda(1-t_1)}\tilde{U}). \qquad [33]$$

Here, U, $e^{-p\Lambda t}$, $\mathcal{B}$, and $\tilde{U}$ are matrix representations in the Laplacian eigenbasis for $\rho(\mathbf{r})$, $G_t(\mathbf{r}, \mathbf{r}')$, $B(\mathbf{r})$, and $\tilde{\rho}(\mathbf{r})$, respectively. As previously, each matrix in this product has a clear interpretation. In fact, the trajectory is started with a given initial density (vector U). During the time interval between 0 and t_1, there is no gradient so that the evolution is described by the matrix $e^{-p\Lambda t_1}$. Then, at time t_1, a nucleus acquires a phase shift (matrix $\mathcal{B}$). After that, no magnetic field is applied between t_1 and 1 which is represented by $e^{-p\Lambda(1-t_1)}$. Finally, the vector $\tilde{U}$ is written to include the pickup function. The first moment is then obtained by integrating $\mathbb{E}\{B(X_{t_1})\}$ with the temporal profile $f(t_1)$ according to Eq. [32].

The reader's attention is directed to the following point. In most practical situations, the pickup function $\tilde{\rho}(\mathbf{r})$ is constant and can be omitted. In this case, the presence of the propagator $G_{1-t_1}(\mathbf{r}_1,\mathbf{r})$ in the above integral form of $\mathbb{E}\{B(X_{t_1})\}$ may seem to be unnecessary. This is actually true for a purely reflecting boundary (without surface relaxation, $h = 0$). Since there is no gradient or other relaxing mechanisms during the time interval $[t_1,1]$, the magnetization does not decay (i.e., the number of excited nuclei is preserved). In other words, the integral of the propagator $G_{1-t_1}(\mathbf{r}_1, \mathbf{r})$ over $\mathbf{r}$ is equal to 1 (probabilistic normalization) and it can thus be omitted. In addition, if the initial density is uniform, one gets $U_m = \delta_{m,0}$ so that

$$\mathbb{E}\{\mathcal{B}(X_{t_1})\} = \mathcal{B}_{0,0}, \qquad [34]$$

independently of time t_1. If the rephasing condition [25] holds, the first moment $\mathbb{E}\{\phi\}$ vanishes. However, this reasoning fails for relaxing boundaries ($h > 0$). In this case, the propagator $G_{1-t_1}(\mathbf{r}_1, \mathbf{r})$ is mandatory to guarantee that the magnetization of nuclei is survived up to the observation time. An omission of this propagator would lead to larger (overestimated) moments and erroneous results. This remark concerns all the moments.

Unexpectedly, a numerical computation of the first moment is more complicated than that of the macroscopic signal. In fact, in the latter case, one needed to compute the matrix product in Eq. [27] only once (for a given set of the physical parameters p, q, and h). In contrast, the time integral in Eq. [32] has to be first approximated by a finite sum, and the matrix product in Eq. [33] has to be calculated for each term in this sum. The computation becomes much harder for higher-order moments that involves an approximation of multiple integrals (see later). Another substantial difference is that the computation of the macroscopic signal, which is based only on matrix products, is very accurate, while that for the moments involves an approximation of the time integral. On the other hand, as shown later, a theoretical

analysis of the moments is much easier than that of the macroscopic signal.

Second Moment

Using similar probabilistic arguments, the second and higher-order moments can be written in a compact matrix form (*1*), e.g.,

$$\mathbb{E}\{\phi^2/2\} = \int_0^1 dt_1 f(t_1) \int_{t_1}^1 dt_2 f(t_2)\, \mathbb{E}\{\mathcal{B}(X_{t_1})\mathcal{B}(X_{t_2})\}. \quad [35]$$

In what follows, the double time integral in Eq. [35] is denoted as $<\ldots>_2$. The two-point correlation function is

$$\mathbb{E}\{\mathcal{B}(X_{t_1})\mathcal{B}(X_{t_2})\} = (U\, e^{-p\Lambda t_1}\, \mathcal{B}\, e^{-p\Lambda(t_2-t_1)} \mathcal{B}\, e^{-p\Lambda(1-t_2)} \tilde{U}). \quad [36]$$

As for the first moment, the probabilistic interpretation of this result is straightforward: starting with a given initial density (vector U), a nucleus experiences the magnetic field (two matrices $\mathcal{B}$) at two successive (random) positions at times t_1 and t_2 along its stochastic trajectory. A diffusive motion between these positions is described by the matrices $e^{-p\Lambda t_1}$, $e^{-p\Lambda(t_2-t_1)}$, and $e^{-p\Lambda(1-t_2)}$. The last matrix ensures that the nucleus survives until the observation time, at which the magnetization is weighted by a sampling function (vector $\tilde{U}$).

A simplification can be achieved when there is no surface relaxation ($h = 0$). When the initial density $\rho(\mathbf{r})$ and the sampling function $\tilde{\rho}(\mathbf{r})$ are uniform, Eq. [29] yields $U_m = \tilde{U}_m = \delta_{m,0}$. The second moment is then equal to the temporal average $<\ldots>_2$ of the first diagonal element of the matrix $\mathcal{B}e^{-p\Lambda(t_2-t_1)}\mathcal{B}$:

$$\mathbb{E}\{\phi^2/2\} = \left\langle \left[\mathcal{B}\, e^{-p\Lambda(t_2-t_1)}\mathcal{B}\right]_{0,0} \right\rangle_2 \quad [37]$$

(throughout the text, the subscript $_{0,0}$ denotes the first diagonal element of a matrix).

As we mentioned earlier, the moments are much more appropriate for theoretical analysis. For instance, Robertson investigated diffusion between two parallel plates by evaluating the second moment (*66*). As a matter of fact, the majority of theoretical studies of restricted diffusion in NMR are focused on the second moment [see (*1*) and references therein]. The reason is twofold.

1. The second moment provides the major contribution to the macroscopic signal for relatively small gradients (small q). In fact, the characteristic function can be expanded into a Taylor series in powers of q up to the second order:

$$E = \mathbb{E}\{e^{iq\phi}\} \simeq 1 + iq\mathbb{E}\{\phi\} - q^2\mathbb{E}\{\phi^2/2\}.$$

This relation can also be written, with the same accuracy, in a more familiar form

$$E \simeq \exp\left[iq\mathbb{E}\{\phi\} - \frac{q^2}{2}\left(\mathbb{E}\{\phi^2\} - [\mathbb{E}\{\phi\}^2\right)\right]. \quad [38]$$

The mean phase $\mathbb{E}\{\phi\}$ determines an oscillating part, while the standard deviation $\mathbb{E}\{\phi^2\} - [\mathbb{E}\{\phi\}]^2$ defines an attenuation. For spin-echo experiments, the rephasing condition [25] cancels the first moment that yields the "Gaussian phase approximation" (GPA)

$$E \simeq \exp[-q^2\mathbb{E}\{\phi^2/2\}]. \quad [39]$$

In many cases, the knowledge of the second moment is enough for a satisfactory description of the macroscopic signal.

2. A technical complexity of the analysis grows rapidly with the moment order. Few theoretical results are known about higher-order moments. Bergman and Dunn developed a formalism for computing the fourth moment in the case of a periodic porous medium (*67*, *68*). Exact analytical expressions for the fourth and sixth moments are derived in (*69*) for the specific case of a cosine magnetic field. The discussion of higher-order moments goes beyond the scope of this article.

Short-Time Diffusion Regime: Leading Term

For a short time T or a small diffusion coefficient D, the average displacement $\sqrt{DT}$ of the spin-bearing particles is small in comparison with the size L of a confining domain: $p = \sqrt{DT}/L \ll 1$. If there is no surface relaxation ($h = 0$), the second moment is given by Eq. [37], in which the exponential function can be formally expanded into a power series up to the first order in p:

$$\mathbb{E}\{\phi^2/2\} \simeq [\mathcal{B}\mathcal{B}]_{0,0}\, \langle 1\rangle_2 - p\langle(t_2 - t_1)\rangle_2 [\mathcal{B}\Lambda\mathcal{B}]_{0,0}, \quad [40]$$

where

$$\langle 1\rangle_2 = \int_0^1 dt_1 f(t_1) \int_{t_1}^1 dt_2 f(t_2) = \frac{1}{2}\left(\int_0^1 dt f(t)\right)^2$$

and

$$\begin{aligned}\langle (t_1 - t_2)\rangle_2 &= \int_0^1 dt_1 f(t_1) \int_{t_1}^1 dt_2 f(t_2)\,(t_1 - t_2) \\ &= \int_0^1 dt \left(\int_0^t dt' f(t')\right)^2 \\ &\quad - \left(\int_0^1 dt\, f(t)\right)\left(\int_0^1 dt \int_0^t dt' f(t')\right).\end{aligned}$$

Under the rephasing condition [25], $\langle 1\rangle_2 = 0$ and

$$\langle (t_1 - t_2)\rangle_2 = \int_0^1 dt \left(\int_0^t dt' f(t')\right)^2. \qquad [41]$$

For a given profile $f(t)$, the computation of this average is straighforward, either analytically (if possible), or numerically. For instance, one finds for a trapezoidal profile from Fig. 4(c):

$$\begin{aligned}\langle (t_1 - t_2)\rangle_2 &= \frac{1}{2}\tau^2 + \tau\delta + \frac{1}{2}\delta^2 - \frac{7}{15}\tau^3 \\ &\quad - \frac{7}{6}\tau^2\delta - \tau\delta^2 - \frac{1}{3}\delta^3.\end{aligned}$$

If the ramp time τ is equal to 0, the trapezoidal profile is replaced by a rectangular one, for which $\langle (t_1 - t_2)\rangle_2 = \delta^2(1/2 - \delta/3)$ (20). When $\delta = 1/2$, one retrieves $\langle (t_1 - t_2)\rangle_2 = 1/12$.

The constant $[\mathcal{B}\Lambda\mathcal{B}]_{0,0}$ can be written in an integral form [see (*1*) for details]:

$$\zeta_1 \equiv [\mathcal{B}\Lambda\mathcal{B}]_{0,0} = \sum_m \mathcal{B}_{0,m} L^2 \lambda_m \mathcal{B}_{m,0} = \frac{L^2}{V}\int_\Omega d\mathbf{r} |\nabla B(\mathbf{r})|^2, \qquad [42]$$

which is equal to 1 for a linear gradient. As a consequence, one finds

$$\mathbb{E}\{\phi^2/2\} \simeq p\langle (t_1 - t_2)\rangle_2. \qquad [43]$$

For weak gradients, the macroscopic signal takes the classical Gaussian form

$$\begin{aligned}E &\simeq \exp[-q^2 p \langle (t_1 - t_2)\rangle_2] \\ &= \exp\left[-D\gamma^2 g^2 T^3 \int_0^1 dt \left(\int_0^t dt'\, f(t')\right)^2\right]. \qquad [44]\end{aligned}$$

This formula becomes exact for free (unrestricted) diffusion as shown by Stejskal and Tanner (*70*). The combination $T_g = (D\gamma^2 g^2)^{-1/3}$ defines a typical time T_g which is needed for a diffusing nucleus to acquire a sufficient phase shift for a considerable signal decay:

$$E \simeq \exp[-(T/T_g)^3 \langle (t_1 - t_2)\rangle_2]. \qquad [45]$$

A faster-then-exponential decay of the macroscopic signal in time is a typical feature of unrestricted diffusion. In section "Long-Time Diffusion Regime," an alteration of this behavior by a geometrical restriction is discussed.

Short-Time Diffusion Regime: Corrections

A careful revision of the above derivation reveals a gross defect. A series expansion of the exponential function in Eq. [37] is not mathematically allowed since higher-order terms $\mathcal{B}\Lambda^2\mathcal{B}$, $\mathcal{B}\Lambda^3\mathcal{B}$, ... are divergent due to an unbounded increase of the elements $\Lambda_{m,m}$ with m. At the same time, this very increase ensures a rapid convergence of the exponential function $\exp[-p(t_2 - t_1)\Lambda]$. Some renormalization should therefore be introduced. One can show that the first correction term to Eq. [43] is not p^2 as one might intuitively expect, but $p^{3/2}$.

A qualitative reason for the 3/2 power is simple. In the short-time regime, only the motion of nuclei near the boundary (within a distance in the order of $\sqrt{DT}$) is restricted. The fraction of these nuclei, forming a thin layer near the boundary, can be estimated as the layer volume, $S\sqrt{DT}$, divided by the total volume V (Fig. 6). As a consequence, one expects to retrieve the results for free diffusion for the nuclei in the bulk, with some boundary correction of the order $(S/V)\sqrt{DT} \propto p^{1/2}$. This correction was accurately calculated by Mitra et al. by using a perturbation theory for a propagator for small p (*71–73*). In general, the second moment for a purely reflecting boundary ($h = 0$) reads as follows (*1*):

$$\mathbb{E}\{\phi^2/2\} = \sum_{k=2}^{\infty} (-1)^k \zeta_{k/2} p^{k/2} \langle -(t_2 - t_1)^{k/2}\rangle_2, \qquad [46]$$

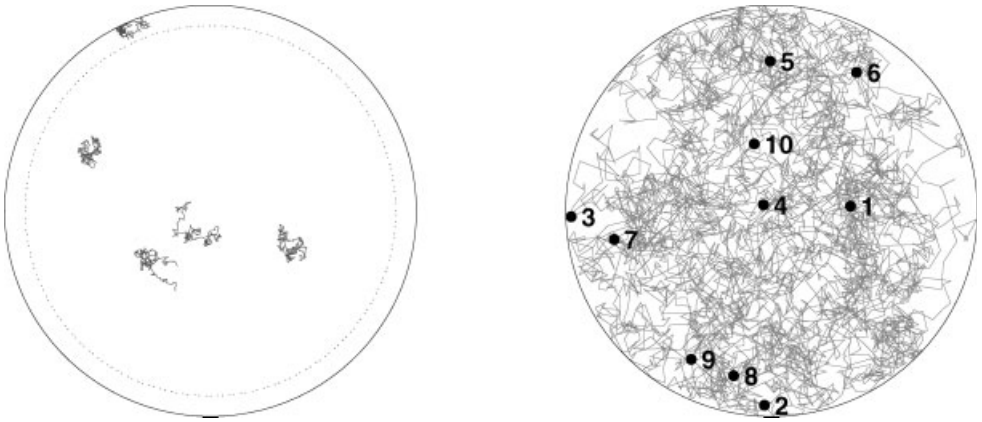

Figure 6 Reflected Brownian trajectories of the nuclei confined inside the unit disk. On the left, five trajectories are drawn in the short-time regime with $p = 0.01$. A dotted inner circle shows the diffusion layer of width $\sqrt{p} = 0.1$. The motion of four nuclei outside the diffusion layer is not restricted. They form the major contribution to the second moment (leading term in the order of p). One nucleus inside the diffusion layer moves slower than the others that modifies its contribution to the second moment (correction term in the order of $p^{3/2}$). On the right, a single trajectory is shown for the long-time regime with $p = 10$. A nucleus explores the bulk of the unit disk several times. Ten black dots show successive positions of the nucleus along its trajectory at times $t_k = kT/10$ ($k = 1,\ldots,10$). Since a nucleus moves fast, these positions look as independent "jumps" to randomly chosen bulk points.

where the coefficients $\zeta_{k/2}$ depend on the geometry of a diffusion-confining domain and on the spatial profile of the magnetic field. The major contribution comes from the term with the coefficient ζ_1 given in Eq. [42], while the first correction is

$$\zeta_{3/2} = \frac{4}{3\sqrt{\pi}} \frac{L^3}{V} \int\limits_{\partial\Omega} d\mathbf{r} \left(\frac{\partial B}{\partial n}\right)^2.$$

For a linear gradient in a given direction $\mathbf{e}$, $\zeta_1 = 1$ and

$$\zeta_{3/2} = \frac{4}{3\sqrt{\pi}} \frac{L}{V} \int\limits_{\partial\Omega} d\mathbf{r} (\mathbf{e} \cdot \mathbf{n}(\mathbf{r}))^2. \qquad [47]$$

The scalar product $(\mathbf{e} \cdot \mathbf{n}(\mathbf{r}))$ is equal to the cosine of the angle between the gradient direction $\mathbf{e}$ and the normal $\mathbf{n}(\mathbf{r})$ to the boundary. When the confining medium is statistically isotropic (i.e., all directions are equivalent), the integral becomes independent (on average) of the gradient direction $\mathbf{e}$, and its computation is reduced to that for rotation-invariant domains such as a disk or a sphere. Then, one gets

$$\zeta_{3/2} = \frac{4}{3\sqrt{\pi}} \frac{L}{V} \frac{S}{d}, \qquad [48]$$

where $1/d$ represents the average over all directions. So, for a linear gradient in statistically isotropic media, the second moment is

$$\mathbb{E}\{\phi^2/2\} \simeq \frac{DT}{L^2} \langle (t_1 - t_2) \rangle_2 \times \left(1 - \frac{4}{3\sqrt{\pi}} \frac{S\sqrt{DT}}{Vd} \frac{\langle (t_2 - t_1)^{3/2} \rangle_2}{\langle (t_2 - t_1) \rangle_2}\right), \qquad [49]$$

where $p = DT/L^2$ is substituted. The correction to the main contribution is of order of $S\sqrt{DT}/V$, while the last ratio in Eq. [49] accounts for the temporal profile used. For instance, for a rectangular two-pulse profile of duration $\delta = 1/2$, one finds

$$\frac{\langle (t_2 - t_1)^{3/2} \rangle_2}{\langle (t_2 - t_1) \rangle_2} = \frac{12(4 - \sqrt{2})}{35},$$

yielding the formula derived in Ref. (*74*). In the limit of very short duration ($\delta \to 0$), one obtains

$$\frac{\langle (t_2 - t_1)^{3/2} \rangle_2}{\langle (t_2 - t_1) \rangle_2} = \frac{1}{\sqrt{2}},$$

and the above formula is reduced to that from Refs. (*71,72*). Some other explicit cases are considered in (*1*). In general, one can easily compute this coefficient for any given temporal profile $F(t)$ by a numerical integration.

Mitra and coworkers suggested to apply Eq. [49] (or its variations) to extract the surface-to-volume ratio S/V of natural and artificial porous media by

measuring the macroscopic signal in the short-time diffusion regime [see (*75*) and references therein]. This equation was repeatedly applied in various contexts. It is worth noting, however, that the form [49] of the short-time behavior is only valid for statistically isotropic media. As discussed in (*1*), Eq. [48] is not applicable even in the case of a parallelepiped, for which the coefficient $\zeta_{3/2}$ should be recalculated according to a more general Eq. [47]. Note that higher-order terms in Eq. [46] can also be significant. In the presence of surface relaxation, the analysis is conceptually the same, but computation is more cumbersome (*60*).

Long-Time Diffusion Regime

In the opposite long-time diffusion regime, the average displacement $\sqrt{DT}$ is much larger than the size L of a confining medium. The confining medium is assumed to be bounded (or "closed") so that none of the spin-bearing particles can enter or escape. This situation should not be confused with another common frame of "open" infinitely large systems, when the whole exploration of a confining medium is never attained [for results in this case, see (*75*) and references therein; see also the related discussion in (*1*)].

In the long-time regime ($p \gg 1$), each nucleus explores the bulk of a bounded confining domain several times. A nucleus moves so fast that its spatial displacements look like independent "jumps" at randomly chosen bulk points (Fig. 6). It means that different nuclei experience an inhomogeneous magnetic field in a similar way, the phenomenon known as motional narrowing or averaging [see (*1*) for details]. The distribution of the phase shifts is therefore expected to be Gaussian and the signal to be given by Eq. [39].

Since p is large, a perturbation theory cannot be applied any more for an analytical computation of the second moment in the long-time regime. In turn, one can use the fact that the parameter p appears in the argument of exponential matrices in Eq. [36]. When matrix products are written explicitly by sums, many terms are exponentially small for $p \gg 1$. The only contribution in time integrals in Eq. [35] appears when $t_2 - t_1$ is small. When there is no surface relaxation ($h = 0$), the general behavior is (*1*)

$$\mathbb{E}\{\phi^2/2\} \simeq \frac{\zeta_{-1}}{p} \int_0^1 dt\, f^2(t) + O(p^{-2}), \qquad [50]$$

where the time integral incorporates the temporal profile $f(t)$, and ζ_{-1} is a geometry-dependent coefficient

$$\zeta_{-1} = \frac{1}{L^2} \sum_{m=1}^{\infty} \mathcal{B}_{0,m} \lambda_m^{-1} \mathcal{B}_{m,0}. \qquad [51]$$

The first calculation of ζ_{-1} for a slab geometry goes back to Robertson who obtained $\zeta_{-1} = 1/120$ (*66*). Eight years later, Neuman performed a computation for a cylinder and a sphere that gave 7/96 and 8/175, respectively (*76*). Neuman also derived the correction of the order of p^{-2} in the case of a rectangular two-pulse temporal profile. As pointed out in (*1*), the main contribution in Eq. [50] is universal, while the form of the correction terms depends on a particular choice of the temporal profile. An analytical computation for slab, cylinder, and sphere with a relaxing boundary ($h > 0$) is given in (*60*).

Under the Gaussian phase approximation, the macroscopic signal is determined by the second moment, yielding

$$E \simeq \exp\left[-\zeta_{-1} \frac{\gamma^2 g^2 L^4 T}{D} \int_0^1 dt\, f^2(t)\right]. \qquad [52]$$

One immediately observes apparent differences between this attenuation and that of the short-time diffusion regime through Eq. [44]:

1. The diffusion coefficient D appears in the denominator: faster diffusion leads to a weaker attenuation. It may look counter-intuitive since faster diffusion yields a stronger mixing of the spin-bearing particles. However, this mixing helps to average out specific contributions of the local magnetization to the macroscopic signal.
2. The logarithm of the signal is proportional to the observation time T, instead of varying as T^3 in the short-time regime (Eq. [45]).
3. The signal is dependent on, and very sensitive to, the size L of a confining medium. In addition, a supplementary geometry-dependent coefficient ζ_{-1} appears.

Further details on the long-time behavior can be found in (*1*).

Apparent Diffusion Coefficient

The second moment of the phase shift can be used to define an effective, time-dependent or, equivalently, apparent diffusion coefficient (ADC):

$$D(p) = D \frac{\mathbb{E}\{\phi^2/2\}}{p\langle (t_1 - t_2)\rangle_2}. \qquad [53]$$

Woessner introduced the above "spin-echo diffusion coefficient" as a measure of fluctuations of the phase shift (*77*). This is the ratio between the second moment $\mathbb{E}\{\phi^2/2\}$ and its value for free (unrestricted) diffusion according to Eq. [43]. ADC shows how geometrical restrictions "slow down" the diffusive dynamics of nuclei (*75*). In the short-time limit ($p \to 0$), one retrieves $D(0) = D$ as expected.

When the Gaussian phase approximation holds, the signal is determined by the second moment so that

$$D(p) = \frac{-\ln E}{q^2 p \langle (t_1 - t_2) \rangle_2 / D}. \qquad [54]$$

The denominator of this formula is often called the *b*-factor, *b*-value or *b*-coefficient:

$$b = \frac{q^2 p}{D} \langle (t_1 - t_2) \rangle_2 \ = \gamma^2 g^2 T^3 \langle (t_1 - t_2) \rangle_2. \qquad [55]$$

This notation leads to a particularly simple form of the signal

$$E = \exp[-bD(p)]$$

that allows one to measure $D(p)$ experimentally as the slope of the dependence of log E versus b-value. As discussed in "How Apparent is Diffusion Coefficient" section, more attention should be paid to the definition and computation of ADC. For instance, the above equation can be used, rigorously speaking, only in the limit of zero b.

If there is no surface relaxation ($h = 0$), Eq. [37] yields

$$D(p) = D \sum_m \underbrace{L^2 \lambda_m \mathcal{B}_{0,m}^2}_{\text{weights}} \overbrace{w_f}^{\text{profile f(t)}} (p \underbrace{\lambda_m}_{\text{time scaling}}), \qquad [56]$$

where the function $w_f(p)$ depends only on the choice of the temporal profile $f(t)$:

$$w_f(p) = \frac{\langle e^{-p(t_2 - t_1)} \rangle_2}{\langle p(t_1 - t_2) \rangle_2}. \qquad [57]$$

The spectral representation [56] states that ADC is simply a superposition of terms which are obtained by rescaling the unique function $w_f(p)$.

The function $w_f(p)$ approaches 1 for small p (its asymptotic behavior can be derived from Eq. [49]), and it behaves as p^{-2} for large p according to Eq. [50]. For instance, if $f(t)$ is a rectangular two-pulse profile of duration $\delta = 1/2$ [Fig. (4a)], one finds $\langle (t_1 - t_2) \rangle_2 = 1/12$ and

$$w_f(p) = 12 \left(\frac{1}{p^2} - \frac{e^{-p} - 4e^{-p/2} + 3}{p^3} \right).$$

For a linear gradient, Eq. [42] yields

$$\sum_m L^2 \lambda_m \mathcal{B}_{0,m}^2 = \zeta_1 = 1.$$

so that each term $L^2 \lambda_m \mathcal{B}_{0,m}^2$ in Eq. [56] can be thought of as a relative weight of the eigenfunction u_m contributing to ADC. In turn, the eigenvalue λ_m determines a characteristic time scale at which the contribution appears in Eq. [56] through the function $w_f(p)$. Eq. [56] allows one to distinguish the roles of various "ingredients" of the problem. So, the spatial profile of the magnetic field enters only into the weights $\lambda_m \mathcal{B}_{0,m}^2$, while the temporal profile is fully taken into account by the function $w_f(p)$. Finally, the geometry determines both the time scales $(D\lambda_m)^{-1}$ and the weights $\lambda_m \mathcal{B}_{0,m}^2$. Equation [56] relates spectral properties of the Laplace operator to measurable characteristics of a diffusion-confining domain. The spectral analysis provides not only a clear and useful interpretation of ADC but also forms a mathematical ground for a more profound analysis. As an example, it is demonstrated in the Appendix that ADC is a decreasing function of time (if there is no surface relaxation). To our knowledge, this is the first rigorous proof of this fact.

Localization Regime

In many cases of practical interest, the knowledge of the second moment is enough for an accurate approximation of the macroscopic signal. However, when the gradient intensity increases, the fourth and higher-order moments become progressively more and more significant. Starting from some gradient intensity, a perturbative approach fails since one needs to calculate too many terms. This problem can be illustrated by the following example. The exponential function e^{-x} can always be expanded into an absolutely convergent power series

$$e^{-x} = \sum_{n=0}^{\infty} \frac{(-x)^n}{n!}.$$

This series can in principle be used to calculate the value of the exponential function for any x. However, the computation with an accuracy better than

1% requires at least 8 terms for $x = 2$ and 14 terms for $x = 3$. The number of terms grows rapidly with x. Moreover, the resulting value of the exponential function becomes smaller with increasing x, while it is calculated by summing up large numbers with opposite signs. The computational error increases dramatically. For instance, such a perturbative computation becomes useless for $x = 10$. The same problem appears for the macroscopic signal, with the "only" complication that the perturbative terms are now the high-order moments $\mathbb{E}\{\phi^n/n!\}$ which are difficult to calculate (*69*).

This problem was studied theoretically by Stoller and co-workers for a slab geometry (*78*). They derived an asymptotic behavior of the macroscopic signal at high gradient intensity:

$$E \propto (p/q)^{1/3} \exp\left[-\frac{a_1}{2}(pq^2)^{1/3}\right], \qquad [58]$$

where $a_1 \simeq 1.0188$ is the absolute value of the first zero of the derivative of the Airy function [the correction factor $(p/q)^{1/3}$ was later introduced by Hürlimann et al. (*79*)]. The stretched exponential behavior [58] can be attributed neither to the short-time regime nor to the long-time regime. Neither Gaussian phase approximation nor apparent diffusion coefficient have meaning in this so-called localization regime.

With the definitions of p and q, the macroscopic signal in Eq. [58] reads as follows

$$E \propto \frac{L_g S}{V} \exp\left[-\frac{a_1}{2}(T/T_g)\right],$$

where $T_g = (D\gamma^2 g^2)^{-1/3}$ and $L_g = (\gamma g/D)^{-1/3}$ are typical time and length which are needed for a diffusing nucleus to acquire a sufficient phase shift for a considerable signal decay. In contrast to Eq. [45], the signal decay is much slower in the localization regime than for free diffusion. A strong gradient destroys the signal from the unrestricted nuclei in the bulk and makes a boundary layer of width L_g to work effectively as a relaxing surface with a characteristic "lifetime" T_g. The prefactor $L_g\ S/V$ accounts for the fraction of nuclei in the boundary layer.

The dependence [58] and its significance for NMR applications were discussed in (*74*). In particular, the coefficient $a_1/2$ was argued to be independent of a confining geometry. An elegant spin-echo experiment by Hürlimann et al. confirmed a breakdown of the GPA and the relevance of the localization regime (*79*). They studied restricted diffusion of water molecules (with $D \simeq 2.3 \times 10^{-9}\mathrm{m^2 s^{-1}}$) between two parallel plates at distance $L = 0.16$ mm. The signal attenuation was measured as a function of the gradient intensity g. Even for gradient pulses of a long duration $T = 120$ ms, the dimensionless diffusion coefficient p was small, $p = 0.01$, so that one could expect to observe the short-time regime with a Gaussian g^2 dependence, Eq. [44]. A spectacular deviation from this behavior was experimentally observed at gradient intensities above 15 mT m^{-1}.

It is crucial to stress that 15 mT m^{-1} is an ordinary gradient intensity which can be easily created in clinical and research MR scanners. Thousand times higher gradients can be generated in modern scanners for material analysis. The localization regime is not a pathological situation at extreme conditions, but it is as ordinary as the classical Gaussian regime. The rarity of theoretical studies and experimental observations of the localization regime is astonishing. It seems that the convenience of using Gaussian phase approximation and a puzzling belief in its applicability prevented scientists to go beyond this classical frame. The interest in non-Gaussian behaviors started recently to grow (*80*, *81*).

The validity of the Gaussian phase approximation is a long-standing problem [see (*1*) and references therein]. A thorough discussion of this problem would need a separate publication. In this article, only limitations of the GPA by a simple numerical example are illustrated. As in Hürlimann et al's. experiment (*79*), restricted diffusion between parallel plates is considered, and the macroscopic signal is computed by using the matrix formalism described in Part 1. For the sake of simplicity, surface relaxation is neglected ($h = 0$). The macroscopic signal E as a function of two dimensionless parameters, q^2 and p, is shown in Fig. 7. When the Gaussian phase approximation holds, the signal, plotted on a logarithmic scale, linearly decreases with q^2 for a fixed p. This behavior is clearly seen for $p = 0.01$ (short-time regime; curve is shown by circles) and $p = 10$ (long-time regime; curve is shown by squares). However, there is a significant deviation from the Gaussian behavior for intermediate values of p. To make the difference clearer, the signal predicted by the GPA is plotted in the same figure. The localization regime is not presented on this plot (e.g., a deviation from the Gaussian behavior in Hürlimann's experiment is started from $g \geq 15$ mT m^{-1} that corresponds to $q^2 \geq 6000$ for the numerical example used). In summary, our example shows the importance of checking the validity of the Gaussian phase approximation in experments, as well as the interest in theoretical and numerical investigation of restricted diffusion beyond this classical regime.

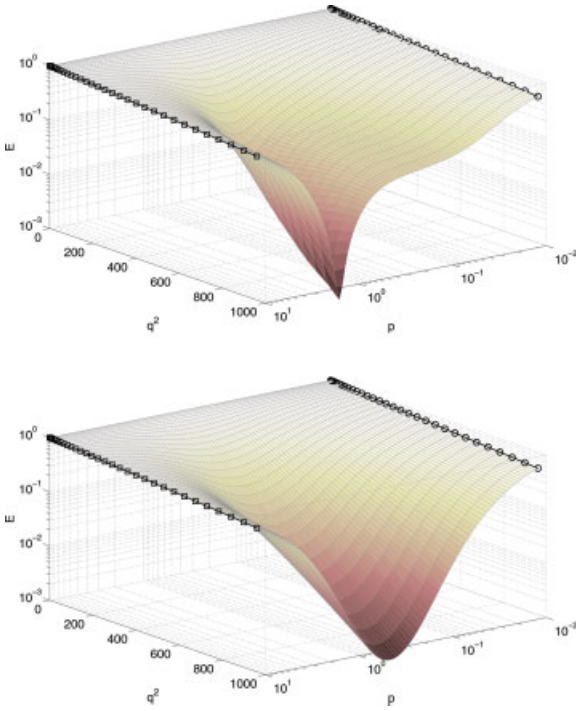

Figure 7 Macroscopic signal from the nuclei diffusing between two parallel plates [a linear magnetic field gradient is applied perpendicularly to these plates; the effective temporal profile used here is shown in Fig. (4a)]. On the top, the signal is plotted as a function of two parameters: square of the dimensionless gradient intensity, $q^2 = (\gamma gTL)^2$, and the dimensionless diffusion coefficient, $p = DT/L^2$ (here, there is no surface relaxation, $h = KL/D = 0$). On the bottom, the signal obtained by the Gaussian phase approximation [39] is plotted. The two curves shown by squares and circles represent the short-time and long-time regimes, for which the second moment is given by Eqs. [49] and [50], respectively. [Color figure can be viewed in the online issue, which is available at www.interscience.wiley.com.]

IV. DISCUSSION

Given a pedagogical character of this article, the Discussion section is organized in the form of answers to some questions that a reader might want to ask after reading previous sections.

Are Simple Shapes of Any Interest?

The power of a spectral description relies on its applicability to any bounded domain. For instance, the structure of the short-time and long-time asymptotic formulas is the same for all the domains, the difference between their shapes appearing in the values of a limited number of constants (including $\zeta_{3/2}$ and ζ_{-1}). At the same time, the computation of these constants and of the macroscopic signal requires finding Laplacian eigenfunctions, at least a part of them. As discussed in Part 1, this is a difficult numerical task. Using a matrix formalism, we "push" all computational problems toward a construction of the matrices Λ and $\mathcal{B}$. Once these matrices are constructed, numerically or analytically, the remaining computation is easy, rapid, and very accurate. In this light, simple diffusion-confining domains for which the eigenfunctions are already known, are particularly useful to "probe" a matrix formalism. In Part 1, explicit formulas for the matrices Λ and $\mathcal{B}$ were given for the unit interval, disk, and sphere with a purely reflecting boundary ($h = 0$). A general case of partially reflecting boundaries was treated in (*1*), in which the values for various geometry-dependent constants were also listed. Since the matrices Λ and $\mathcal{B}$ are known explicitly for these simple shapes, a spectral-oriented computation is particularly efficient.

A practical importance for considering simple shapes is a possibility to use them for testing numerical tools. For instance, what is the appropriate size for truncation of the infinite-dimensional matrices Λ and $\mathcal{B}$? How does the accuracy vary with the truncation size? How many eigenfunctions is needed? It is much easier to answer these questions for simple shapes, for which there is almost no limitation in the number of eigenfunctions that can be calculated.

The results for simple shapes are often presented as "illustrations" for all bounded domains. These illustrations may, however, lead to a dangerous oversimplification of the problem. Although many concepts of restricted diffusion are valid both for simple and complicated shapes, a "blind" illustration may be misleading. Two examples are given.

1. As shown in (*1*), the elements of the matrix $\mathcal{B}$ for three simple shapes (interval, disk, sphere) are fully expressed in terms of the eigenvalues λ_m. The eigenfunctions u_m "disappear" from the scene as though they are irrelevant to the problem. This is a very particular feature of these three shapes and of a linear magnetic field gradient. When one modifies the magnetic field or considers other domains, the eigenfunctions are essential.
2. The considered simple shapes have one geometric length scale, i.e., their size L. For instance, one could clearly distinguish the short-time and long-time regimes by comparing L with the diffusion length $\sqrt{DT}$. In contrast, many porous structures (lungs, cement,

sedimentary rock, etc.) exhibit multiple length scales. If ℓ and L are the smallest and the largest length scales of a domain, there may emerge new features in the intermediate region $\ell \ll \sqrt{DT} \ll L$. For instance, the emergence of a "tortuosity" regime for thin circular and spherical layers is shown, which exhibit two length scales, is shown in (*61*).

The consequences of the multiscale character of porous media on restricted diffusion are still poorly understood. For instance, the role of connectivity is unclear (*82*). The roughness of a boundary is expected to be important for certain time scales (*83*, *84*). All these questions require a substantial study of restricted diffusion in complex geometries.

What Is an Analytical Solution?

With currently available computational facilities, a question of distinction between the scopes of theoretical and numerical analysis arises stronger than ever. What is "an analytical solution" of a problem, and what is it used for? At first thought, this question may appear strange or ridiculous. From a classical point of view, an analytical solution is expressed in terms of "elementary" functions (e.g., powers, exponential or sine functions) or, more generally, of "special" functions (e.g., Bessel functions). However, even an exponential function needs a numerical computation to be evaluated. Even if a simple analytical solution were available, we still need a computer for getting numbers that can be compared with experimental values. Is it really different from a numerical solution of a problem? To make our concerns clearer, two examples are considered.

1. Two formulas can be compared for the macroscopic signal attenuation in a linear magnetic field gradient: Eq. [44] which is exact for unrestricted diffusion in the whole space, and Eq. [27] for restricted diffusion for a slab. The first formula is a typical example of an analytical solution, which eventually is very simple. The second formula, involving infinite-dimensional matrices (with explicitly known elements), is not classified as an analytical solution in the classical sense. However, the conceptual difference between these formulas is superficial. In fact, both formulas are exact and explicit, they involve the exponential function and clearly reveal the dependence on physical parameters. Both formulas require a computer to get the signal for a given set of physical parameters. Finally, in both cases, the computation is easy, rapid, and very accurate (if matrices are not too big). Our favor for the first formula relies on a preference to deal with the exponential function of a number rather than that of a matrix.
2. The second example was suggested by Barzykin who showed that the macroscopic signal attenuation due to diffusion in a linear gradient in a slab can be expressed as an integral of a hypergeometric function (*85*). This is an example of an analytical solution in the classical sense. Although analytical, this expression is of very limited use, for both numerical and theoretical purposes. In contrast, the matrix representation [27] of the same signal is instructive for theoretical considerations and efficient for numerical computation, though this form is not classified as an analytical solution.

A classical view on an analytical solution as a tabulated function should be revised. The new criteria for a solution to be considered as analytical may be the following: rapidity, ease and robustness of computation, clarity of its physical interpretation, usefulness for practical applications. A matrix formalism satisfies all these criteria.

Does One Need a Theoretical Analysis?

In Part 1, an efficient numerical tool for calculating the macroscopic signal is described. Having this tool in hand, one may wonder what is the interest in further theoretical advances? In other words, if the signal can be found very accurately in a numerical way, should one really care about sophisticated asymptotic techniques, Laplace transforms, and multiple integrals which would allow one to get approximate solutions with a limited range of applicability? In our opinion, this question should bother any theoretician because in some cases the derived asymptotic results are not worth the efforts to get them. Let us however describe at least three situations in which theoretical results remain invaluable.

1. A numerical computation may become inaccurate in some limiting cases. For instance, a numerical computation of a diffusive propagator in the short-time limit requires a large number of eigenfunctions. Even in the simplest case of the unit interval, for which everything is known explicitly, and the eigenfunctions are particularly simple (sine and

cosine functions), a direct summation in Eq. [20] fails for times smaller than 0.01 because of round-off errors. In fact, the asymptotic formula [21] indicates that $G_t(0,1) \simeq e^{-1/(4t)}/\sqrt{4\pi t} \simeq 4 \times 10^{-11}$ for $t = 0.01$ (we put dimensionless units here, with $D = 1$). The difficulty is now evident: in Eq. [20], we are summing up terms of the order of 1 in attempt to compute a very small sum (we evoked a similar problem in the section "Localization Regime"). While a numerical computation becomes worse as t is getting smaller, the asymptotic formula [21] becomes more and more accurate. The numerical and theoretical analysis are complementary in this situation.

2. Theoretical analysis allows one to ensure and sometimes to control the convergence of numerical results. For instance, the theory states that the macroscopic signal exhibits a multi-exponential attenuation [31] due to surface relaxation. It is therefore possible to estimate the required number of terms and the truncation error. Another example is a computation of the second moment in the short-time regime. The asymptotic formula [46] allows one to keep several first terms and to omit the others, for which one can estimate an error.
3. A numerical computation works as a "black box" which produces results without giving "explanations." In fact, physical parameters appear explicitly in the matrix form, but the resulting macroscopic signal depends on them in a very complicated way because of a matrix exponential. Theoretical analysis allows one to shed a light onto this dependence and to explain why this or that behavior is observed. For instance, a matrix formalism correctly reproduces an exponential decay [52] of the macroscopic signal in the long-time regime, but it neither explains it nor allows one to relate the constant ζ_{-1} to the spectral properties and the geometry of a diffusion-confining domain. This is the purpose of theoretical analysis.

What Can One Do in Porous Media?

Although simple shapes are useful for theoretical analysis, main "targets" of DWI have much more complicated geometrical structures. The geometry of biological tissues, human organs, mineral samples, and materials is complex in many ways, in particular:

1. These structures exhibit multiple length scales (*86*, *87*). For instance, the architecture of sedimentary rocks can be represented by interconnected rough channels with a spread pore size distribution (*64*, *65*). A broad range of length scales makes questionable the use of a single dimensionless diffusion coefficient p.
2. The boundary of these media is often irregular that may considerably influence the signal attenuation, either by diffusional screening [inhomogeneous accessibility for diffusing particles, see (*15–22*, *88*)] or by enhancing susceptibility-induced magnetic field gradients [see (*89*) and references therein].

It is then natural to ask whether a spectral approach can be used for describing restricted diffusion in porous media. As we mentioned earlier, the spectral approach is formally applicable to any bounded domain, whatever its complexity is. Most theoretical results remain valid in general [e.g., the short-time asymptotic behavior of the macroscopic signal which assesses the surface-to-volume ratio of a diffusion-confining medium (*71–73*, *75*)]. The central problem for using a spectral approach in practice is a numerical computation of the governing matrices Λ and $\mathcal{B}$ that is a real challenge in the case of complex geometries. For this purpose, some model structures of porous media (like hierarchical morphologies, self-similar fractals, ordered or random packs of spherical beads, etc.) are of great interest. Some kind of statistical averaging may possibly be required for reducing information about irrelevant geometrical details. A better understanding of spectral characteristics of the Laplace operator in complex domains and of its consequences for restricted diffusion in porous media is an exciting area for future research.

Is a Porous Medium Bounded or Open?

A broad range of length scales suggests to consider porous media as infinite unbounded systems. This consideration relies on a very simple principle: if the majority of diffusing nuclei cannot reach the frontier of a sample during an experiment, it does not matter whether this frontier exists or not. The motion of nuclei is then modeled as unrestricted diffusion with an apparent diffusion coefficient which accounts for the presence of geometrical obstacles, paramagnetic impurities, sinks, traps, etc. This approach is helpful in many practical situations, especially when a numerical computation of Laplacian eigenfunctions for the whole system is too challenging. In some cases it is convenient to describe a macroscopically homoge-

neous medium as periodic (*67*, *68*, *90–93*). In particular, diffusion eigenstates can be introduced and used to investigate the macroscopic signal (*93*).

In this article, it is not going to be argued whether a porous medium is worth to be considered as bounded or unbounded. Either approach has its own advantages and drawbacks, and the choice between them strongly depends on the problem in hand. At present, applications of spectral tools were mainly restricted to simple shapes, but this situation may change in future.

How Apparent Is Diffusion Coefficient?

As discussed in "Apparent Diffusion Coefficient" section, an apparent diffusion coefficient is measured as a slope of log E versus b-value in the limit of zero b. ADC contains potentially useful information about translational dynamics of nuclei and about the geometry of a diffusion-confining domain. The relative simplicity and noninvasive character of diffusion-weighted NMR measurements made ADC a broadly used characteristics of porous media, from lung and brain imaging in medicine (*41*, *42*) to sedimentary rock analysis in oil recovery industry (*86*, *94*).

It seems that a routine use of ADC erased the frontiers of its application. It is important to recall some "traps" to which a blind use of ADC may lead.

1. A magnetic field is applied to measure the signal so that $D(p)$ incorporates its effect. In particular, the short-time and long-time asymptotic formulas [49, 50] for the second moment (and thus for ADC) explicitly depend on the temporal and spatial profiles of the magnetic field. ADC is therefore not an intrinsic characteristic of a medium: two distinct measurements of ADC on the same sample may lead to different results. As a consequence, the information extracted from a spin-echo ADC cannot be considered independently of measurement conditions. The reported ADC values should be accompanied by an accurate specification of an experimental setup (gradient intensity and waveform, timing, etc.). The simplicity of using a single b-value for a combination of physical parameters is tempting, but it is a dangerous oversimplification.
2. $D(p)$ is not in general equivalent to the classical time-dependent diffusion coefficient that characterizes the mean square displacement in time: $D_{\mathrm{msd}}(t) = \mathbb{E}\{[\mathbf{r}(t) - \mathbf{r}(0)]^2\}/6t$. The distinction becomes particularly pronounced in the long-time regime. In a bounded domain, the mean square displacement approaches a constant so that $D_{\mathrm{msd}}(t) \propto 1/t$. In turn, in section "Apparent Diffusion Coefficient" it is seen that $D(p) \propto 1/p^2 \propto 1/t^2$.
3. ADC is supposed to be a function of a dimensionless time $p(=DT/L^2)$, while the right-hand side of Eq. [54] is a priori function of p and q. The notion of ADC is therefore only meaningful when the Gaussian phase approximation holds. As discussed in "Localization Regime" section, the GPA may break down at ordinary experimental conditions. In this situation (e.g., for the localization regime), ADC has no meaning. In practice, it is important to measure the macroscopic signal at several gradient intensities g and then to check that ADC is indeed independent of g.

What Does Diffusion Tell Us about Geometry?

In this article, a forward problem which consists in predicting transport properties of a system with a given (or known) geometry is considered. The central question here is: "How does the macroscopic signal depend on physical parameters (gradient strength, observation time, etc.) for a given diffusion-confining domain?". This question is of fundamental interest. In practice, however, one is often interested in solving an inverse problem which consists in determining an unknown geometry by monitoring restricted diffusion. So, DWI aims at extracting information about the geometry of a diffusion-confining medium from measurements of the macroscopic signal as a function of physical parameters. Moreover, geometrical information should be revealed at length scales which are smaller than the available spatial resolution (size of voxels) that can be achieved by gradient encoding. For instance, the spatial resolution of gas DWI of human lungs is of the order of a millimeter, while one needs to extract information about the acinar structure at submillimetric scales (*40–42*). In other words, we want to say something about the geometry of a diffusion-confining domain inside a single spatial voxel. All the information that we have in our hands is the macroscopic signal, and how the signal depends on physical parameters. This inverse problem is a great challenge. After realizing the complexity of the problem, one may wonder whether it is solvable at all. A full recovery of an unknown geometry seems to be unrealistic, both from mathematical and physical points of view.

From a mathematical point of view, the macroscopic signal is fully determined by the governing matrices Λ and $\mathcal{B}$ which, in turn, are formed by the Laplacian eigenfunctions and the spatial profile $B(\mathbf{r})$ of the magnetic field. Does the structure of the matrices Λ and $\mathcal{B}$ determine the shape? This question goes back to the famous Kac's question "Can one hear the shape of a drum?" (*95*). In fact, the acoustic frequences that we hear from a drum are given by the eigenvalues of the Laplace operator which depend on the shape of a drum. If we know all the eigenvalues (i.e., the matrix Λ), do we know the geometry? The negative answer to this question was given by Gordon et al. who constructed isospectral domains of different shapes (*96*). It means that the matrix Λ alone cannot determine the shape. In NMR, we have a freedom to choose the encoding magnetic field $B(\mathbf{r})$ that provides us with another matrix $\mathcal{B}$. One may therefore ask whether it is possible to define such a function $B(\mathbf{r})$ so that the knowledge of the related matrix $\mathcal{B}$ would determine the shape of a diffusion-confining domain. If a full recovery is still impossible, what would be the "best" choice for the function $B(\mathbf{r})$ to extract as much information as we can? To our knowledge, these challenging mathematical questions are open.

From a physical point of view, even if a full recovery of the shape was possible in principle, an unavoidable presence of noise would certainly limit its practical implementation. For instance, if we measure the signal attenuation due to surface relaxation, we can in principle determine the spectral information from Eq. [31]. However, this equation contains an infinity of terms whose contributions exponentially decay as m increases. The presence of unavoidable noise limits our abilities to recover the spectral information to several most significant terms in this sum.

If we focus on a partial recovery of the shape, many useful results can be achieved. For instance, the surface-to-volume ratio of a porous medium can be determined in the short-time limit (''Short-Time Diffusion Regime: Corrections'' section). In some cases, one can extract pore size distribution ("Zeroth Moment" section). Recent progress with correlation experiments (e.g., combined measurement of T_1–T_2 relaxation times) opens new ways for characterizing restricted diffusion (*97–100*). Further discussion goes beyond the scope of this article.

V. CONCLUSIONS

Surprisingly, the role of Laplacian eigenfunctions in NMR is often underestimated. On one hand, it is so natural to think of diffusion problems in terms of Laplacian eigenfunctions that it is difficult to trace back who suggested it first. On the other hand, a numerical computation of eigenfunctions was a challenging problem for a long time. With limited computational facilities, one naturally preferred to search for a single solution of the Bloch-Torrey equation for specific initial and boundary conditions instead of looking for numerous eigenfunctions. The lack of efficient "eigensolver" led to a broadly accepted point of view that spectral tools are worth only for simple shapes, for which the eigenfunctions are known explicitly. This point of view has to be reconsidered nowadays.

First, Laplacian eigenfunctions form a mathematical ground for a thorough theoretical analysis of restricted diffusion which can be applied to any bounded domain, simple or complex. The two governing matrices Λ and $\mathcal{B}$ completely determine restricted diffusion and the consequent macroscopic signal. The spectral approach is a general and well-adapted mathematical language to speak about restricted diffusion, at both theoretical and numerical levels. In particular, the short-time and long-time asymptotic results are universal. Many results about restricted diffusion can be proved by using spectral decompositions.

Second, computational facilities are progressively increasing. Of course, the geometry of many biological and mineral systems is still too complicated for a numerical computation of eigenfunctions. However, here we are not speaking about solving diffusion problems for such systems on supercomputers is not being spoken of. What is more important is to understand the mechanism how a complex geometry influences the macroscopic signal. For this purpose, one can start with model shapes like self-similar fractals or packs of spherical beads, for which finding Laplacian eigenfunctions is more tractable. Since diffusing particles have no memory, diffusion is not very sensitive to specific geometrical details. Once the role of a geometrical complexity is understood for model shapes, similar mechanisms are expected to work for realistic shapes. This will be a new step in understanding restricted diffusion and its role in NMR.

ACKNOWLEDGMENTS

The author is thankful to Dr. M. Hürlimann and Dr. D. Tchelkak for fruitful discussions concerning the decrease of the time-dependent diffusion coefficient. A proofreading by T. Iakovleva is gratefully acknowledged. The author thanks both referees for their helpful remarks and suggested improvements.

APPENDIX

Time-Dependent Diffusion Coefficient

Here, the use of a spectral analysis is illustrated by showing that the time-dependent diffusion coefficient $D(p)$ is a decreasing function of time (if there is no surface relaxation). To our knowledge, this is the first rigorous proof of this result. Although the presented demonstration may look too technical for a pedadogical article, it illustrates well the potential applications of spectral tools.

The demonstration relies on the spectral representation [56] for $D(p)$. First of all, it is reminded that this representation was deduced from Eq. [40] by assuming that the rephasing condition [25] holds. In this case, the temporal average $\langle (t_1 - t_2) \rangle_2$ is given by Eq. [41] and it is strictly positive. This condition is important: e.g., if $f(t)$ was equal to 1, one would get $\langle (t_1 - t_2) \rangle_2 = -1/6$.

If $w_f(p)$ is shown to be a decreasing function, then $D(p)$ should decrease as being a sum of decreasing functions with positive coefficients $\lambda_m \mathcal{B}_{0,m}^2$. The derivative of $w_f(p)$ is as follows:

$$w_f'(p) = -\frac{\langle e^{-p(t_2-t_1)}[p(t_2-t_1)+1] \rangle_2}{p^2 \langle (t_1-t_2) \rangle_2}$$

The denominator of this ratio is positive due to the rephasing condition. Our aim is to show that the numerator is also positive for any temporal profile $f(t)$, that is as follows:

$$\int_0^1 dt_1 \int_0^1 dt_2 f(t_1) f(t_2) K(t_1, t_2) \geq 0, \qquad [A1]$$

$$K(t_1, t_2) = e^{-p|t_2-t_1|}(p|t_2 - t_1| + 1).$$

In other words, it has to be shown that an integral operator defined by the kernel $K(t_1, t_2)$ is positively definite for any $p > 0$ (for $p = 0$, one gets $w_f'(0) = 0$). This integral operator is defined on the space L^2 ([0,1]) of measurable and square integrable functions on the unit interval. Let us consider another integral operator defined by the same kernel but on a larger space $L^2(\mathbb{R})$. The Fourier transform of the kernel of this operator is calculated as follows:

$$\int_{\mathbb{R}} dt\, e^{i\omega t} e^{-p|t|}(p|t| + 1) = \frac{4p^3}{(p^2 + \omega^2)^2} > 0.$$

The last inequality implies that this operator is positively definite: for any $f \in L^2(\mathbb{R})$,

$$\int_{\mathbb{R}} dt_1 \int_{\mathbb{R}} dt_2 f(t_1) f(t_2) K(t_1, t_2) \geq 0. \qquad [A2]$$

As $L^2([0,1]) \subset L^2(\mathbb{R})$, the original integral operator is also positive definite that proves inequality [A1] and $w_f'(p) < 0$. This completes the proof that $w_f(p)$ is a decreasing function.

REFERENCES

1. Grebenkov DS. 2007. NMR survey of reflected Brownian motion. Rev Mod Phys 79:1077–1137.
2. Grebenkov DS. 2008. Laplacian eigenfunctions in NMR. I. A numerical tool. Conc Magn Reson A 32:277–301.
3. Brown R. 1828. A brief account of microscopical observations made in the months of June, July and August, 1827, on the particles contained in the pollen of plants; and on the general existence of active molecules in organic and inorganic bodies. Edinburgh N Phil J 5:358–371.
4. Feller W. 1971. An Introduction to Probability Theory and Its Applications, 2nd ed., Volumes I and II. New York: Wiley.
5. Bouchaud JP, Georges A. 1990. Anomalous diffusion in disordered media: statistical mechanisms, models and physical applications. Phys Rep 195:127–293.
6. Shlesinger MF, Klafter J, Zumofen G. 1999. Above, below and beyond Brownian motion. Am J Phys 67:1253–1259.
7. Metzler R, Klafter J. 2000. The random walk's guide to anomalous diffusion: a fractional dynamics approach. Phys Rep 339:1–77.
8. Havlin S, ben Avraham D. 2002. Diffusion in disordered media. Adv Phys 51:187–292.
9. Kimmich R. 2002. Strange kinetics, porous media, and NMR. Chem Phys 284:253–285.
10. Spitzer F. 1976. Principles of Random Walk. New York: Springer.
11. Weiss GH. 1994. Aspects and Applications of the Random Walk. Amsterdam: North-Holland.
12. Hughes BD. 1995. Random Walks and Random Environments. Oxford: Clarendon.
13. Freidlin M. 1985. Functional Integration and Partial Differential Equations. Annals of Mathematics Studies. Princeton, New Jersey: Princeton University.
14. Grebenkov DS, Filoche M, Sapoval B. 2003. Spectral properties of the Brownian self-transport operator. Eur Phys J B 36:221–231.
15. Sapoval B. 1994. General formulation of Laplacian transfer across irregular surfaces. Phys Rev Lett 73:3314–3317.

16. Filoche M, Sapoval B. 1999. Can one hear the shape of an electrode? II. Theoretical study of the Laplacian transfer. Eur Phys J B 9:755–763.
17. Grebenkov DS, Filoche M, Sapoval B, Felici M. 2005. Diffusion-reaction in branched structures: theory and application to the lung acinus. Phys Rev Lett 94:050602.
18. Grebenkov DS, Lebedev AA, Filoche M, Sapoval B. 2005. Multifractal properties of the harmonic measure on Koch boundaries in two and three dimensions. Phys Rev E 71:056121.
19. Felici M, Filoche M, Straus C, Similowski T, Sapoval B. 2005. Diffusional screening in real 3D human acini—a theoretical study. Resp Physiol Neurobiol 145:279–293.
20. Grebenkov DS, Filoche M, Sapoval B. 2006. Mathematical basis for a general theory of Laplacian transport towards irregular interfaces. Phys Rev E 73:021103.
21. Grebenkov DS. 2006. Partially reflected Brownian motion: a stochastic approach to transport phenomena. In: Velle LR, ed. Focus on Probability Theory. Hauppauge: Nova Science Publishers. pp 135–169.
22. Grebenkov DS. 2006. Scaling properties of the spread harmonic measures. Fractals 14:231–243.
23. Redner S. 2001. A Guide to First-Passage Processes. Cambridge, England: Cambridge University Press.
24. Bossy M, Gobet E, Talay D. 2004. A symmetrized Euler scheme for an efficient approximation of reflected diffusions. J Appl Prob 41:877–889.
25. Burdzy K, Chen ZQ. 2008. Discrete approximations to reflected Brownian motion. Ann Probab 36:698–727.
26. Hahn EL. 1950. Spin echoes. Phys Rev 80:580–594.
27. Carr HY, Purcell EM. 1954. Effects of diffusion on free precession in NMR experiments. Phys Rev 94:630–638.
28. Biswas RR, Sen PN. 2007. Taylor dispersion with absorbing boundaries: a stochastic approach. Phys Rev Lett 98:164501.
29. Callaghan PT. 1991. Principles of Nuclear Magnetic Resonance Microscopy. Oxford: Clarendon.
30. Grebenkov DS. 2007. Residence times and other functionals of reflected Brownian motion. Phys Rev E 76:041139.
31. Torrey HC. 1956. Bloch equations with diffusion terms. Phys Rev 104:563–565.
32. Kac M. 1949. On the distribution of certain Wiener functionals. Trans Am Math Soc 65:1–13.
33. Kac M. 1951. On some connections between probability theory and differential and integral equations. In: Proceedings of the 2nd Berkeley Symposium Mathematical Statistics and Probability. Neyman J ed. Berkeley: University of California Press. pp 189–215.
34. Darling DA, Kac M. 1957. On occupation times for Markoff processes. Trans Am Math Soc 84:444–458.
35. Tanner JE, Stejskal EO. 1968. Restricted self-diffusion of protons in colloidal systems by the pulsed-gradient, spin-echo method. J Chem Phys 49:1768–1777.
36. Callaghan PT, Coy A, MacGowan D, Packer KJ, Zelaya FO. 1991. Diffraction-like effects in NMR diffusion studies of fluids in porous solids. Nature (London) 351:467–469.
37. Price WS. 1997. Pulsed-field gradient nuclear magnetic resonance as a tool for studying translational diffusion, Part 1. Basic theory. Conc Magn Reson 9:299–336.
38. Price WS. 1998. Pulsed-field gradient nuclear magnetic resonance as a tool for studying translational diffusion, Part 2. Experimental aspects. Conc Magn Reson 10:197–237.
39. Callaghan PT, Codd SL, Seymour JD. 1999. Spatial coherence phenomena arising from translational spin motion in gradient spin echo experiments. Conc Magn Reson 11:181–202.
40. Möller HE, Chen XJ, Saam B, Hagspiel KD, Johnson GA, Altes TA, de Lange EE, Kauczor HU. 2002. MRI of the lungs using hyperpolarized noble gases. Magn Reson Med 47:1029–1051.
41. van Beek EJR, Wild JM, Kauczor HU, Schreiber W, Mugler JP III, de Lange EE. 2004. Functional MRI of the lung using hyperpolarized 3-helium gas. J Magn Reson Imag 20:540–554.
42. Conradi MS, Saam B, Yablonskiy DA, Woods JC. 2006. Hyperpolarized 3He and perfluorocarbon gas diffusion MRI of lungs. Prog Nucl Magn Reson Spectrosc 48:63–83.
43. Blees MH. 1994. The effect of finite duration of gradient pulses on the pulsed-field-gradient NMR method for studying restricted diffusion. J Magn Res A 109:203–209.
44. Mitra PP, Halperin BI. 1995. Effects of finite gradient pulse widths in pulsed field gradient diffusion measurements. J Magn Reson A 113:94–101.
45. Wang LZ, Caprihan A, Fukushima E. 1995. The narrow-pulse criterion for pulsed-gradient spin-echo diffusion measurements. J Magn Reson A 117:209–219.
46. Mair RW, Sen PN, Hürlimann MD, Patz S, Cory DG, Walsworth RL. 2002. The narrow pulse approximation and long length scale determination in xenon gas diffusion NMR studies of model porous media. J Magn Reson 156:202–212.
47. Zielinski LJ, Sen PN. 2003. Effects of finite-width pulses in the pulsed-field gradient measurement of the diffusion coefficient in connected porous media. J Magn Reson 165:153–161.
48. Birman MS, Solomyak MZ. 1987. Spectral Theory of Self-Adjoint Operators in Hilbert Space. Dordrecht: D. Reidel Publishing Company.
49. Bass RF. 1998. Diffusions and Elliptic Operators. New York: Springer.
50. Lapidus ML. 1991. Fractal drum, inverse spectral problems for elliptic operators and a partial resolu-

tion of the Weyl-Berry conjecture. Trans Am Math Soc 325:465–529.
51. Song YQ. 2000. Detection of the high eigenmodes of spin diffusion in porous media. Phys Rev Lett 85:3878–3881.
52. Lisitza NV, Song YQ. 2001. The behavior of diffusion eigenmodes in the presence of internal magnetic field in porous media. J Chem Phys 114:9120–9124.
53. Lisitza NV, Song YQ. 2002. Manipulation of the diffusion eigenmodes in porous media. Phys Rev B 65:172406.
54. Weiss GH. 1986. Overview of theoretical models for reaction rates. J Stat Phys 42:3–36.
55. Torquato S, Avellaneda M. 1991. Diffusion and reaction in heterogeneous media: pore-size distribution, relaxation times, and mean survival time. J Chem Phys 95:6477–6489.
56. Torquato S. 1991. Diffusion and reaction among traps: some theoretical and simulation results. J Stat Phys 65:1173–1206.
57. Brownstein KR, Tarr CE. 1979. Importance of classical diffusion in NMR studies of water in biological cells. Phys Rev A 19:2446–2453.
58. Carslaw HS, Jaeger JC. 1959. Conduction of heat in solids, 2nd ed. Oxford: Clarendon.
59. Crank J. 1975. The Mathematics of Diffusion, 2nd ed. Oxford: Clarendon.
60. Grebenkov DS. 2007. Multiple correlation function approach: rigorous results for simple geometries. Diff Fundam 5:1–34.
61. Grebenkov DS. 2008. Analytical solution for restricted diffusion in circular and spherical layers in inhomogeneous magnetic fields. J Chem Phys 128:134702.
62. Grebenkov DS. 2006. Multiexponential attenuation of the CPMG spin echoes due to a geometrical confinement. J Magn Reson 180:118–126.
63. Giorgi T, Smits RG. 2005. Monotonicity results for the principal eigenvalue of the generalized Robin problem. Illin J Math 49:1133–1143.
64. Kleinberg RL. 1994. Pore size distributions, pore coupling, and transverse relaxation spectra of porous rocks. Magn Reson Imag 12:271–274.
65. Latour LL, Kleinberg RL, Mitra PP, Sotak CH. 1995. Pore-size distributions and tortuosity in heterogeneous porous media. J Magn Reson A 112:83–91.
66. Robertson B. 1966. Spin-echo decay of spins diffusion in a bounded region. Phys Rev 151:273–277.
67. Bergman DJ, Dunn KJ. 1995. NMR of diffusing atoms in a periodic porous medium in the presence of a nonuniform magnetic field. Phys Rev E 52:6516–6535.
68. Dunn KJ, Bergman DJ. 1995. Self diffusion of nuclear spins in a porous medium with a periodic microstructure. J Chem Phys 102:3041–3054.
69. Grebenkov DS. 2007. NMR restricted diffusion between parallel planes in a cosine magnetic field: an exactly solvable model. J Chem Phys 126:104706.
70. Stejskal EO, Tanner JE. 1965. Spin diffusion measurements: spin echoes in the presence of a time-dependent field gradient. J Chem Phys 42:288–292.
71. Mitra PP, Sen PN, Schwartz LM, Le Doussal P. 1992. Diffusion propagator as a probe of the structure of porous media. Phys Rev Lett 68:3555–3558.
72. Mitra PP, Sen PN, Schwartz LM. 1993. Short-time behavior of the diffusion coefficient as a geometrical probe of porous media. Phys Rev B 47:8565–8574.
73. Axelrod S, Sen PN. 2001. Nuclear magnetic resonance spin echoes for restricted diffusion in an inhomogeneous field: methods and asymptotic regimes. J Chem Phys 114:6878–6895.
74. de Swiet TM, Sen PN. 1994. Decay of nuclear magnetization by bounded diffusion in a constant field gradient. J Chem Phys 100:5597–5604.
75. Sen PN. 2004. Time-dependent diffusion coefficient as a probe of geometry. Conc Magn Reson A 23:1–21.
76. Neuman CH. 1974. Spin echo of spins diffusion in a bounded medium. J Chem Phys 60:4508–4511.
77. Woessner DE. 1963. NMR spin-echo self-diffusion measurements on fluids undergoing restricted diffusion. J Phys Chem 67:1365–1367.
78. Stoller SD, Happer W, Dyson FJ. 1991. Transverse spin relaxation in inhomogeneous magnetic fields. Phys Rev A 44:7459–7477.
79. Hürlimann MD, Helmer KG, de Swiet TM, Sen PN, Sotak CH. 1995. Spin echoes in a constant gradient and in the presence of simple restriction. J Magn Reson A 113:260–264.
80. Jacob RE, Laicher G, Minard KR. 2007. 3D MRI of non-Gaussian 3He gas diffusion in the rat lung. J Magn Reson 188:357–366.
81. Grebenkov DS, Guillot G, Sapoval B. 2007. Restricted diffusion in a model acinar labyrinth by NMR. Theoretical and numerical results. J Magn Reson 184:143–156.
82. Grebenkov DS, Guillot G. 2007. NMR of diffusion in porous media: branched or disordered structure? Magn Reson Imag 25:560.
83. Sapoval B, Russ S, Petit D, Korb JP. 1996. Fractal geometry impact on nuclear relaxation in irregular pores. Magn Reson Imag 14:863–867.
84. Stallmach F, Vogt C, Karger J, Helbig K, Jacobs F. 2002. Fractal geometry of surface areas of sand grains probed by pulsed field gradient NMR. Phys Rev Lett 88:105505.
85. Barzykin AV. 1999. Theory of spin echo in restricted geometries under a step-wise gradient pulse sequence. J Magn Reson 139:342–353.
86. Song YQ, Ryu S, Sen PN. 2000. Determining multiple length scales in rocks. Nature (London) 406:178–181.
87. Sahimi M. 1993. Flow phenomena in rocks: from continuum models to fractals, percolation, cellular

automata, and simulated annealing. Rev Mod Phys 65:1393–1534.
88. Levitz PE, Grebenkov DS, Zinsmeister M, Kolwankar K, Sapoval B. 2006. Brownian flights over a fractal nest and first passage statistics on irregular surfaces. Phys Rev Lett 96:180601.
89. Song YQ. 2003. Using internal magnetic fields to obtain pore size distributions of porous media. Conc Magn Reson A 18:97–110.
90. Sen PN, Schwartz LM, Mitra PP, Halperin BI. 1994. Surface relaxation and the long-time diffusion coefficient in porous media: periodic geometries. Phys Rev B 49:215–225.
91. Bergman D, Dunn KJ. 1994. Theory of diffusion in a porous-medium with applications to pulsed-field gradient NMR. Phys Rev B 50:9153–9156.
92. Bergman D, Dunn KJ, Schwartz LM, Mitra PP. 1995. Self-diffusion in a periodic porous medium —a comparison of different approaches. Phys Rev E 51:3393–3400.
93. Bergman DJ. 1997. Diffusion eigenstates of a porous medium with interface absorption. Phys Rev E 55:4235–4244.
94. Hürlimann MD, Helmer KG, Latour LL, Sotak CH. 1994. Restricted diffusion in sedimentary rocks. Determination of surface-area-to-volume ratio and surface relaxivity. J Magn Reson A 111:169–178.
95. Kac M. 1966. Can one hear the shape of a drum? Am Math Monthly 73:1–23.
96. Gordon C, Webb DL, Wolpert S. 1992. One cannot hear the shape of a drum. Bull Am Math Soc 27:134–138.
97. Callaghan PT, Godefroy S, Ryland BN. 2003. Diffusion-relaxation correlation in simple pore structures. J Magn Reson 162:320–327.
98. McDonald PJ, Korb JP, Mitchell J, Monteilhet L. 2005. Surface relaxation and chemical exchange in hydrating cement pastes: a two-dimensional NMR relaxation study. Phys Rev E 72:011409.
99. Washburn KE, Callaghan PT. 2006. Tracking pore to pore exchange using relaxation exchange spectroscopy. Phys Rev Lett 97:175502.
100. Song YQ, Zielinski L, Ryu S. 2008. Two-dimensional NMR of diffusion systems. Phys Rev Lett 100:248002.

BIOGRAPHY

Denis S. Grebenkov received two PhD degrees, the first in statistical physics from the Saint Petersburg State University (Russia) in 2003; and the second in theoretical physics from the Ecole Polytechnique (France) in 2004. He did post-graduate researches on lung imaging at the University Paris-XI (France), and on nonequilibrium dynamics of granular media at the University of Naples (Italy). In 2006, he got a permanent research position at the Laboratory of Condensed Matter Physics, CNRS -- Ecole Polytechnique (France). His main research subject is restricted diffusion in complex geometries.